

# Notes for the MIT NUPAX Oral Exam: Detector Physics

Siddharth Narayanan, MIT

Last modified: May 13, 2016

Disclaimer: the author of these notes makes no guarantee that anything in here is remotely correct.

## Contents

<b>0</b>	<b>General information</b>	<b>4</b>
0.1	Momentum measurement of charged particles . . . . .	4
<b>1</b>	<b>Basic radiation sources</b>	<b>5</b>
<b>2</b>	<b>Passage of radiation through matter</b>	<b>7</b>
2.1	Energy loss of heavy charged particles in matter . . . . .	7
2.2	Cerenkov radiation . . . . .	9
2.3	Interactions of electrons/positrons in matter . . . . .	9
2.3.1	Multiple Coulomb scattering . . . . .	11
2.4	Interaction of photons in matter . . . . .	11
2.4.1	Photoelectric effect . . . . .	11
2.4.2	Compton scattering . . . . .	12
2.4.3	Pair production . . . . .	13
2.4.4	Photon interaction summary . . . . .	15
2.4.5	EM showers . . . . .	15
2.5	Interactions of neutrons in matter . . . . .	16
2.5.1	Mechanisms of interaction . . . . .	16
2.5.2	Neutron moderation . . . . .	17
<b>3</b>	<b>General characteristics of detectors</b>	<b>17</b>
<b>4</b>	<b>Ionization detectors</b>	<b>17</b>
4.1	Types of gaseous ionization detectors . . . . .	17
4.1.1	Resistive plate chamber . . . . .	18
4.1.2	Ionization chamber . . . . .	18
4.1.3	Proportional counter . . . . .	19
4.1.4	Geiger-Müller counter . . . . .	19
4.2	Ionization and transport in gas . . . . .	19
4.2.1	Mean number of $e^-$ /ion pairs . . . . .	19
4.2.2	Recombination and $e^-$ -attachment . . . . .	20
4.2.3	Diffusion . . . . .	20
4.3	Avalanche multiplication . . . . .	20
4.4	Pulse formation and shape . . . . .	21
4.5	Multiwire proportional chamber . . . . .	22
4.6	Drift chamber . . . . .	23
4.7	Time projection chamber . . . . .	24
<b>5</b>	<b>Scintillators</b>	<b>25</b>
5.1	Organic scintillators . . . . .	26
5.2	Inorganic crystals . . . . .	27
5.3	Gas . . . . .	27
5.4	Pulse shape discrimination for particle ID . . . . .	27
5.5	Quenching . . . . .	28
5.6	Electron detection . . . . .	28
5.7	Photon detection . . . . .	28
5.8	Neutron detection . . . . .	28

<b>6</b>	<b>Photomultipliers</b>	<b>29</b>
6.1	Photocathode . . . . .	29
6.2	Multiplier dynodes . . . . .	29
6.3	Gain and voltage supply . . . . .	29
6.4	Pulse shape . . . . .	30
6.5	Time resolution and response . . . . .	30
6.5.1	Geometry of PMT . . . . .	30
6.5.2	Noise . . . . .	30
<b>7</b>	<b>Semiconductor detectors</b>	<b>31</b>
7.1	Basic principles . . . . .	31
7.2	Doped semiconductors . . . . .	32
7.3	The np junction and depletion zone . . . . .	33
7.4	Semiconductors as detectors . . . . .	34
7.4.1	Reverse bias . . . . .	35
7.4.2	Detector characteristics . . . . .	35
7.5	Silicon strip detectors . . . . .	35
7.6	Silicon photomultipliers . . . . .	36
<b>8</b>	<b>Compact Muon Solenoid</b>	<b>36</b>
8.1	Silicon tracker . . . . .	37
8.1.1	Inner pixel detector . . . . .	37
8.1.2	Outer strip detector . . . . .	38
8.1.3	Track reconstruction . . . . .	38
8.1.4	Vertex reconstruction . . . . .	39
8.2	Electromagnetic calorimeter . . . . .	39
8.2.1	Barrel configuration . . . . .	40
8.2.2	Endcap configuration . . . . .	40
8.2.3	Electron and photon reconstruction . . . . .	40
8.2.4	Energy resolution . . . . .	41
8.3	Hadron calorimeter . . . . .	41
8.3.1	HCAL Barrel . . . . .	41
8.3.2	HCAL Endcap . . . . .	42
8.3.3	HCAL Forward . . . . .	42
8.3.4	HCAL Outer . . . . .	42
8.3.5	Jet energy resolution . . . . .	42
8.4	Magnet and return yokes . . . . .	43
8.5	Muon detectors . . . . .	43
8.5.1	Drift tubes . . . . .	43
8.5.2	Resistive plate chambers . . . . .	44
8.5.3	Cathode strip chambers . . . . .	44
8.5.4	Muon reconstruction . . . . .	44
8.6	Triggering and DAQ . . . . .	45
	<b>Appendices</b>	<b>46</b>
<b>A</b>	<b>Bibliography</b>	<b>46</b>

## 0 General information

A barn is  $10^{-24} \text{ cm}^2$ . Consider an incident flux  $F$  on a point target (assuming the width of the beam is larger than the target). The differential cross-section is:

$$\frac{d\sigma}{d\Omega}(E, \Omega) = \frac{1}{F} \frac{dN_{\text{scatt.}}}{d\Omega} \left[ \frac{1}{N/\text{area}} \times \frac{N}{\text{solid angle}} \right] \quad (1)$$

Given a flux  $F$  incident on a target of area  $A$ , numberdensity  $n$ , and thickness  $\delta x$ , the number scattered is:

$$N_{\text{scatt.}} = n \cdot A \cdot F \cdot \delta x \cdot \frac{d\sigma}{d\Omega} \quad (2)$$

The probability-per-unit length for an interaction in matter is:

$$\mu = \sigma \cdot N_A \rho / A \quad (3)$$

where  $A$  is the atomic mass The natural lifetime is  $\tau = \tau_{1/2} / \ln 2$ .

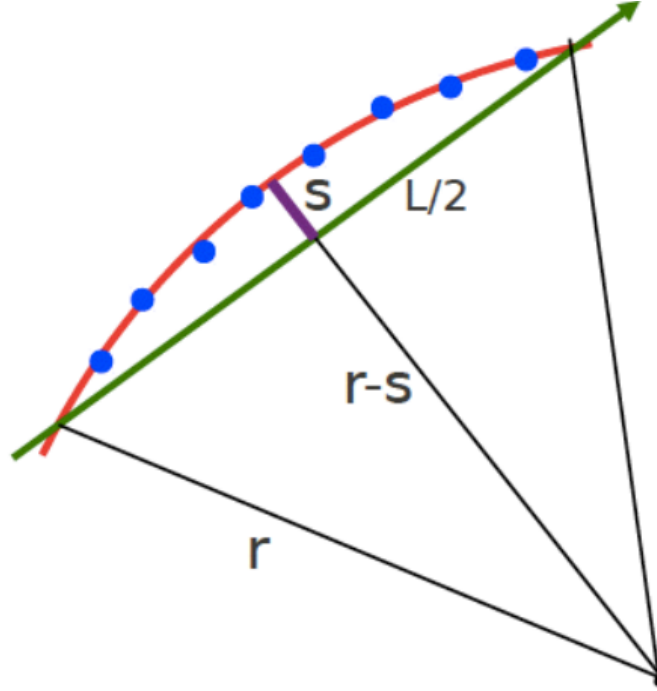
Timing resolution of various detector types:

**Table 33.1:** Typical resolutions and deadtimes of common charged particle detectors. Revised November 2011.

Detector Type	Intrinsic Spatial Resolution (rms)	Time Resolution	Dead Time
Resistive plate chamber	$\lesssim 10 \text{ mm}$	1 ns (50 ps <sup>a</sup> )	—
Streamer chamber	$300 \mu\text{m}^b$	2 $\mu\text{s}$	100 ms
Liquid argon drift [7]	$\sim 175\text{--}450 \mu\text{m}$	$\sim 200 \text{ ns}$	$\sim 2 \mu\text{s}$
Scintillation tracker	$\sim 100 \mu\text{m}$	100 ps/ $n^c$	10 ns
Bubble chamber	10–150 $\mu\text{m}$	1 ms	50 ms <sup>d</sup>
Proportional chamber	50–100 $\mu\text{m}^e$	2 ns	20–200 ns
Drift chamber	50–100 $\mu\text{m}$	2 ns <sup>f</sup>	20–100 ns
Micro-pattern gas detectors	30–40 $\mu\text{m}$	< 10 ns	10–100 ns
Silicon strip	pitch/(3 to 7) <sup>g</sup>	few ns <sup>h</sup>	$\lesssim 50 \text{ ns}^h$
Silicon pixel	$\lesssim 10 \mu\text{m}$	few ns <sup>h</sup>	$\lesssim 50 \text{ ns}^h$
Emulsion	1 $\mu\text{m}$	—	—

### 0.1 Momentum measurement of charged particles

- Typically done by bending the particle in a  $\vec{B}$ -field perpendicular to the direction of motion
- CMS, for example, has a solenoid that causes helical paths
- In general, the path of a particle looks like:



- We can estimate  $R \approx L^2/2s$ .
- The momentum is then  $p_T$  [GeV] =  $0.3 \times B$  [T]  $\times R$  [m]
- There are two sources of uncertainty: measurement and multiple scattering

– Measurement is:

$$\frac{\sigma_{\text{meas.}}}{p_T} = \frac{8\sigma_s}{0.3BL^2} p_T, \quad \sigma_s \propto \frac{\sigma_{r\phi}}{\sqrt{N+4}} \quad (4)$$

Note the uncertainty is larger for high-momentum particles (the track is straighter)

– Multiple scattering is:

$$\frac{\sigma_{\text{MS}}}{p_T} = \frac{0.045}{B} \sqrt{\frac{L}{X_0}} \quad (5)$$

– The use of denser materials and a shorter tracker increases the MS component of the uncertainty

## 1 Basic radiation sources

- $\alpha$ -decay:  $(Z, A) \rightarrow (Z - 2, A - 4) + \alpha$ 
  - Can be thought of as tunneling through nuclear potential
  - $\Rightarrow$  narrow energy range ( $\sim 4 - 6$  MeV)
  - Higher energy  $\Rightarrow$  higher tunneling probability. Therefore, most  $\alpha$ -decays are to the ground state (highest  $\Delta E$ )
  - Large charge:  $\alpha$  particles only pass through few cm of air
- $\beta$ -decay:  $n \rightarrow p + e^- + \bar{\nu}$ ,  $p \rightarrow n + e^+ + \nu$ 
  - Because 3-body decay, there is a continuous spectrum for  $e$  energy
  - Typically goes to an excited nuclear state which decays by  $\gamma$ -radiation

- Electron capture:  $p + e^- \rightarrow n + \nu$ 
  - \* Observed by looking for  $\gamma$  from  $e^-$  filling hole left by captured  $e^-$
- For tritium, the beta particle energy is  $< 20$  keV
- $\gamma$ -emission: nucleus de-excites, emitting a  $\gamma$ 
  - Selection rules: needs to be  $\Delta S = 1$
  - $\mathcal{O}(0.1 - 1)$  MeV
  - Typically happens quickly, but sometimes the transition is spin-suppressed (i.e. if need two  $\gamma$ s to get desired  $\Delta S = 2$  and  $\Delta S = 1$  state is higher energy)
  - Spin-suppressed  $\Rightarrow$  lifetimes up to  $\mathcal{O}(1)$  years
- Annihilation:  $e^- + e^+ \rightarrow 2\gamma$ , (511 keV each)
  - $e^+$  from a  $\beta^+$  process, which interacts with  $e^-$  in absorber or detector
  - Signature is sharp peak at  $E_\gamma = 511$  keV. Photons are emitted back-to-back typically
- Internal conversion: like  $\gamma$ -emission, but energy from nuclear de-excitation goes to an atomic  $e^-$  instead
  - $e^-$  is ejected from shell
  - Typically  $K$ -shell electron
  - Useful source of monoenergetic electrons for calibration
- Neutron sources:  $(Z, A) \rightarrow (Z_1, A_1) + (Z_2, A_2) + n + n + \dots$ 
  - Fission products will undergo  $\beta, \gamma$  decay themselves
  - $$\frac{dN}{dE} = \sqrt{E} \exp \left[ -\frac{E}{T} \right] \tag{6}$$

where  $E$  = energy of neutron,  $T$  = characteristic energy for that decay  $\sim$  MeV
  - Above is for *spontaneous* fission (i.e. no extra energy added to nucleus to cause fission)
- Nuclear reactions:  $A + \alpha \rightarrow B + n$  or  $A + \gamma \rightarrow B + n$ 
  - e.g.  $\alpha + {}^9\text{Be} \rightarrow {}^{13}\text{C}^*$ , where  $C^*$  decays by  $n, \alpha$  or  $3\alpha + n$
  - Typically get  $\mathcal{O}(100)$  neutrons per  $10^6$  as, depending on the source
  - Neutron energy gets smeared quite a bit in decay

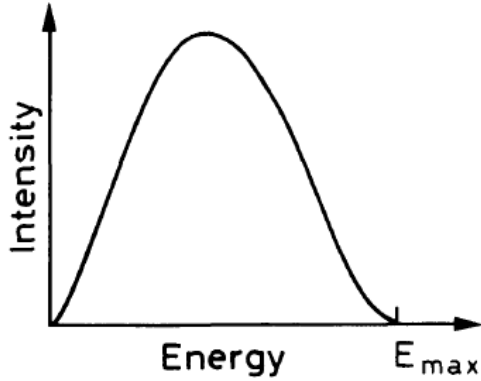


**Fig. 1.2.** Typical continuous energy spectrum of beta decay electrons

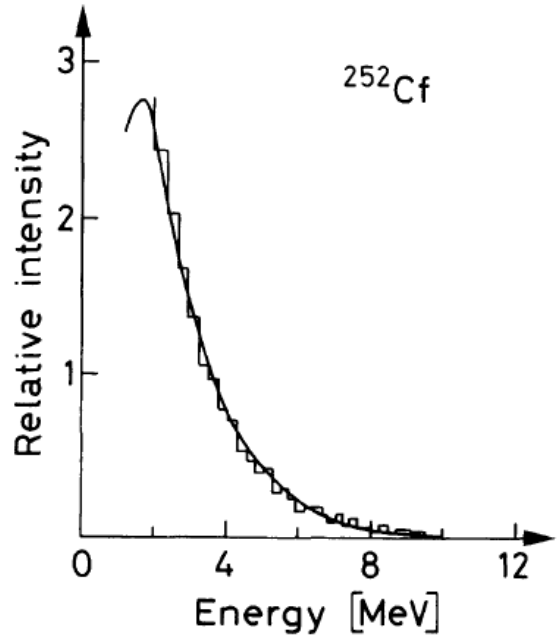


**Fig. 1.5.** Neutron energy spectrum from  $^{252}\text{Cf}$  (from *Lorch et al.* [1.2]). The form of the spectrum can be described by a Maxwellian distribution

## 2 Passage of radiation through matter

- The probability of at least one interaction over a distance  $x$  is  $P(x) = 1 - \exp[-n\sigma x]$ , where  $n$  is the number density of targets

–  $\Rightarrow$  mean free path  $\lambda = 1/n\sigma$

### 2.1 Energy loss of heavy charged particles in matter

- Anything heavier than  $m_e$
- Interactions are with atomic  $e^-$  primarily:  $\sigma \sim 10^7$ - $10^8$  b
- Either excite (soft) or eject (hard) the  $e^-$ 
  - $e^-$  from hard interactions can cause secondary ionization
- Quantity of interest is  $-\langle dE/dx \rangle$ , assuming large fluctuations are very unlikely (untrue for  $e$ )
- Bohr's classical calculation:
  - Assuming the impact parameter between the charged particle (charge  $z$ ) moving at velocity  $v$  and the  $e^-$  is  $b$ :

$$\begin{aligned}
 I &= \frac{2ze^2}{bv} \Rightarrow \Delta E(b) = \frac{I^2}{2m_e} = \frac{2z^2e^4}{m_e v^2 b^2} \\
 \Rightarrow -\frac{dE}{dx} &= \frac{4\pi z^2 e^4}{m_e v^2} N_e \ln \frac{\gamma^2 m v^3}{z e^2 \bar{v}}
 \end{aligned} \tag{7}$$

- where  $\bar{\nu}$  is the average frequency of bound state electrons.
- The value of  $dE/dx$  is gotten by integrating over a reasonable range for  $b$
- Valid for very heavy particles (like  $\alpha$ ), but not for protons, etc, because quantum effects

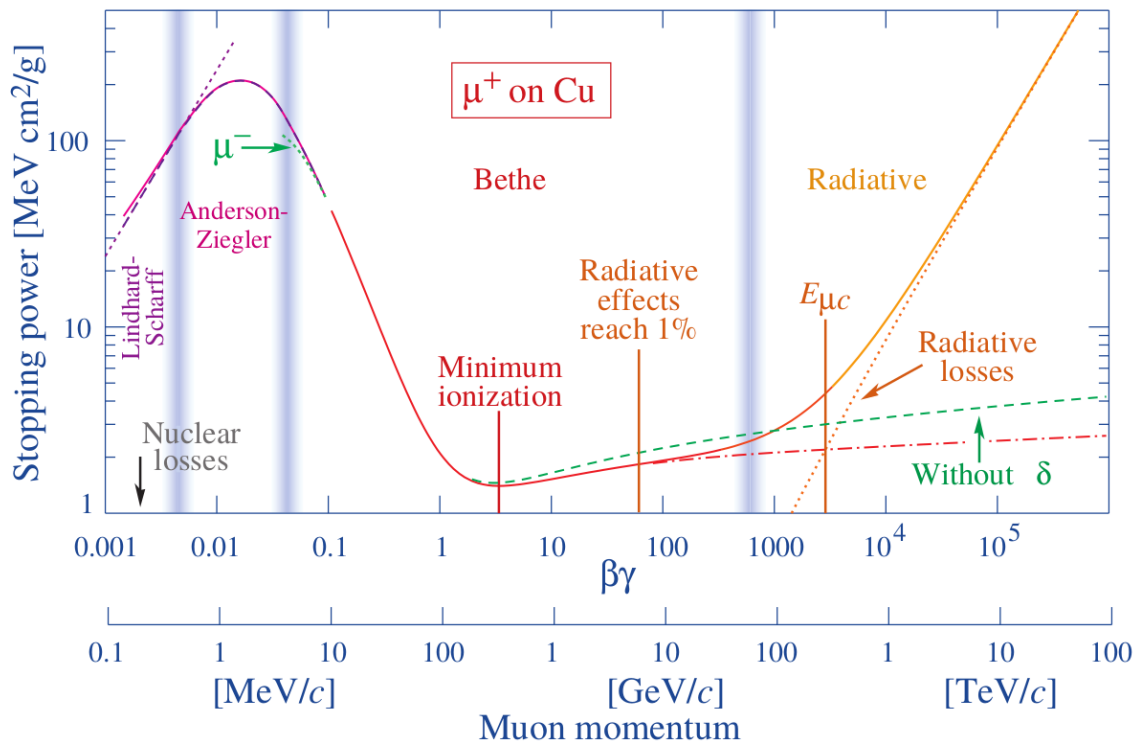
- Bethe-Bloch:

–

$$-\left\langle \frac{dE}{dx} \right\rangle \propto \rho \frac{Z}{A} \frac{z^2}{\beta^2} \left[ \ln \left( \frac{2m_e \gamma^2 \beta^2 W_{\max}}{I^2} \right) - 2\beta^2 - \delta - 2\frac{C}{Z} \right] \quad (8)$$

where:

- \*  $W_{\max}$  is the maximum energy transfer kinematically allowed
- \*  $I$  is the mean excitation potential (material-dependent)
- \*  $\delta$  is the density correction (at high  $\beta$ ). Corrects for the charged particle polarizing the medium as it travels through (stronger effect for high density). This cancels the quadratic rise from the  $\beta^2$  term
- \*  $C/Z$  is the shell-effect. Corrects for case when the incident particle is slow relative to the electron orbital velocity
- Important features:
  - \* Minimum ionizing particle occurs at  $\beta \sim 0.96 \Rightarrow \gamma \sim 3.6$  (independent of the particle)
  - \*  $dE/dx$  goes down as a function of  $\beta$  at low energies: slow particles feel atomic electric field for longer
  - \* But then the  $\beta^2$  relativistic effect causes a rise at high energies: Lorentz contraction of  $\vec{E}$ -field makes transverse component (wrt particle motion) larger.
  - \* The quadratic rise in  $\beta$  is canceled by the  $\delta$  ionization term. Cancellation is stronger for denser materials.





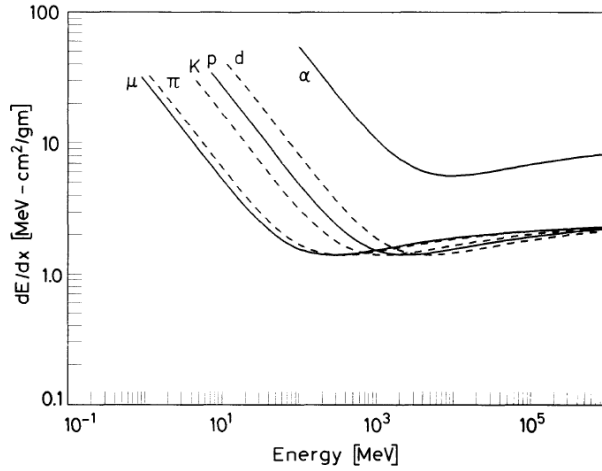


**Fig. 2.4.** The stopping power  $dE/dx$  as function of energy for different particles

- Note that the particle is more ionizing at low  $E \Rightarrow$  more ionization occurs at end of path

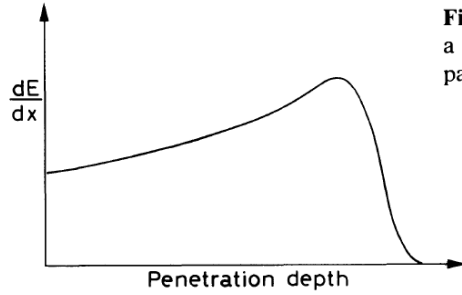


**Fig. 2.5.** A typical Bragg curve showing the variation of  $dE/dx$  as a function of the penetration depth of the particle in matter. The particle is more ionizing towards the end of its path

- For a fixed medium:

$$* \quad \frac{dE}{dx} = z^2 f(\beta)$$

- \*  $\Rightarrow$  if  $\frac{dE}{dx}$  is known for one particle, it is known for all particles (just have to scale  $z^2$  and calculate new  $\beta$  as a function of energy, mass)

## 2.2 Cerenkov radiation

- Speed of light in medium is  $c/n$
- If  $\beta > 1/n$ , a cone of light is observed at an angle  $\theta_C$
- $\cos \theta_C = (\beta n(\nu))^{-1}$  ( $\nu$  is the frequency of the radiation)
- The energy loss is:

$$\begin{aligned}
 -\frac{dE}{dx} &= z^2 \frac{\alpha \hbar}{c} \int d\nu \left[ \nu \left( 1 - (\beta n(\nu))^{-2} \right) \right] \\
 &\iff \\
 \frac{d^2 N_\gamma}{d\nu dx} &= \frac{z^2 \alpha}{c} \left( 1 - (\beta n(\nu))^{-2} \right)
 \end{aligned} \tag{9}$$

## 2.3 Interactions of electrons/positrons in matter

- Bremsstrahlung becomes dominant at  $E > E_c \sim \mathcal{O}(10)$  MeV. Below this, collisions are dominant (described by Bethe-Bloch)

- Bremsstrahlung cross-section is  $\propto (e^2/m)^2 \Rightarrow$  for particles with high  $m$ , bremsstrahlung doesn't become relevant until very very high  $E$ 
  - Kicks in at lower  $E$  for  $e^\pm$

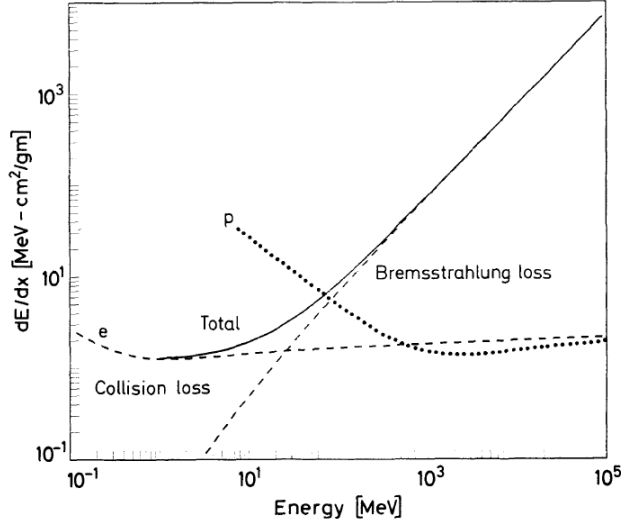


**Fig. 2.10.** Radiation loss vs. collision loss for electrons in copper. For comparison, the  $dE/dx$  for protons is also shown

- $E_c$  is defined as the energy at which  $dE/dx$  due to collision and brem are the same. An empirical formula is:

$$E_c = \frac{800 \text{ MeV}}{Z + 1.2} \quad (10)$$

- For muons,  $E_c$  is  $\sim$  TeV (for low  $Z$ ) to  $\sim$  100 GeV (high  $Z$ )
- Radiation length: distance over a particle's energy is reduced by  $1/e$ . Call it  $L_{\text{rad}}$ 
  - $E = E_0 \exp[-x/L_{\text{rad}}]$

**Table 2.2.** Critical energies of some materials

Material	Critical energy [MeV]
Pb	9.51
Al	51.0
Fe	27.4
Cu	24.8
Air (STP)	102
Lucite	100
Polystyrene	109
NaI	17.4
Anthracene	105
H <sub>2</sub> O	92

**Table 2.3.** Radiation lengths for various absorbers

Material	[gm/cm <sup>2</sup> ]	[cm]
Air	36.20	30050
H <sub>2</sub> O	36.08	36.1
NaI	9.49	2.59
Polystyrene	43.80	42.9
Pb	6.37	0.56
Cu	12.86	1.43
Al	24.01	8.9
Fe	13.84	1.76
BGO	7.98	1.12
BaF <sub>2</sub>	9.91	2.05
Scint.	43.8	42.4

Typical values for  $X_0$ ,  $E_c$  and  $R_M$  of materials  
used in calorimeter

	$X_0$ [cm]	$E_c$ [MeV]	$R_M$ [cm]
Pb	0.56	7.2	1.6
Scintillator (Sz)	34.7	80	9.1
Fe	1.76	21	1.8
Ar (liquid)	14	31	9.5
BGO	1.12	10.1	2.3
Sz/Pb	3.1	12.6	5.2
PB glass (SF5)	2.4	11.8	4.3

- Because of low mass, variance in  $dE/dx$  is larger for  $e^\pm$  than for heavier particles (long tail from large energy transfers)

### 2.3.1 Multiple Coulomb scattering

- Elastic scattering off nuclei
- Very little energy loss since  $m_A \gg m$  typically
- Rutherford formula:

$$\frac{d\sigma}{d\Omega} = z^2 Z^2 \left( \frac{\alpha \hbar c}{T} \right)^2 \frac{1}{\sin^4(\theta/2)} \quad (11)$$

- $T$  is the kinetic energy
- Largest probability for small deflections

- Multiple ( $N_{\text{scatt.}} > 20$ ) scatterings can be treated statistically
  - Assume  $P(\theta)$  is Gaussian centered at 0 (this ignores large deflections in the tails)
  - $\langle \theta^2 \rangle \sim 10^{-3} \text{ rad}^2$  for typical materials
  - Not valid for  $e^\pm$  which have low mass  $\Rightarrow$  large deflections (like backscattering) possible

## 2.4 Interaction of photons in matter

### 2.4.1 Photoelectric effect

- $\gamma + \text{atom} \rightarrow \text{ion} + e^-$
- $E_e = h\nu - \phi$ ,  $\phi$  is the binding energy
- $\sigma$  decreases as  $h\nu$  increases, with a jump up when  $h\nu$  reaches a shell binding energy
- $\sigma \sim \mathcal{O}(10^{-1} - 10^4) \text{ b}$  and is proportional to  $Z^\alpha$ , for  $\alpha = 4 - 5$  (exact value is a function of  $h\nu$ )

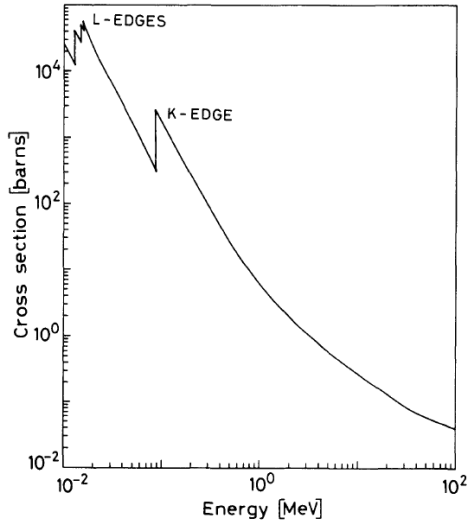


**Fig. 2.21.** Calculated photoelectric cross section for lead

#### 2.4.2 Compton scattering

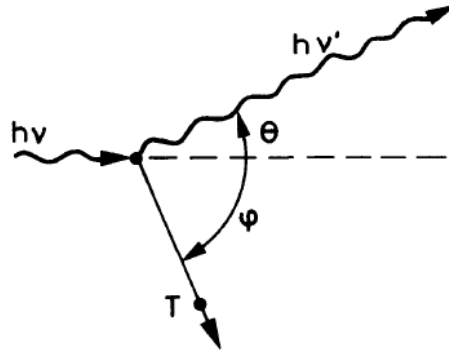


**Fig. 2.22.** Kinematics of Compton scattering

- Kinematics

$$\lambda' - \lambda = \frac{1}{\nu'} - \frac{1}{\nu} = \frac{h}{m_e} (1 - \cos \theta)$$

$$\cot \phi = \left(1 + \frac{h\nu}{m_e}\right) \tan \frac{\theta}{2}$$

- Klein-Nishina:

$$\frac{d\sigma}{d\Omega} = \frac{\alpha^2}{2m_e^2} \left(\frac{\nu'}{\nu}\right)^2 \left[\frac{\nu'}{\nu} + \frac{\nu}{\nu'} - \sin^2 \theta\right] \quad (12)$$

$$\sigma \sim 10^{-4} - 10^0 \text{ b}$$

- Can define  $\sigma_S$  ( $\sigma_A$ ) as the cross-section of scattered (absorbed) energy:

$$\frac{d\sigma_S}{d\Omega} = \frac{h\nu'}{h\nu} \frac{d\sigma}{d\Omega}, \quad \sigma_A = \sigma - \sigma_S \quad (13)$$

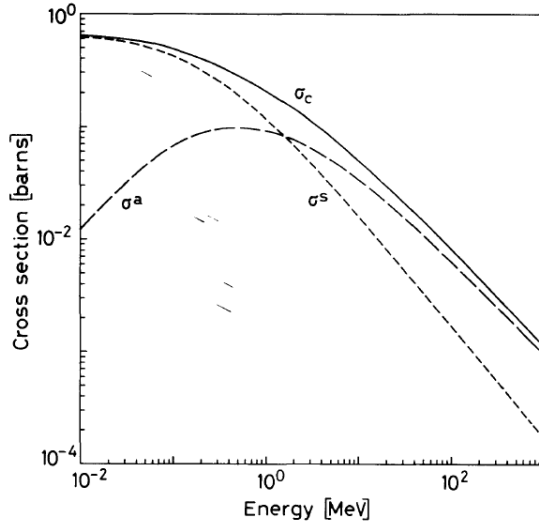


**Fig. 2.23.** Total Compton scattering cross sections

- Can also define  $d\sigma/dT$ , where  $T$  is the kinetic energy of  $e^-$ :

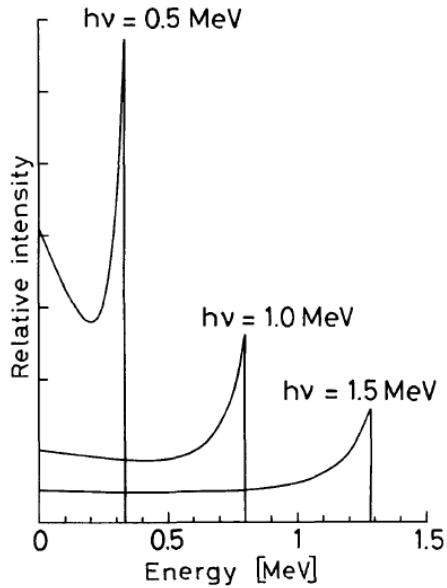


**Fig. 2.24.** Energy distribution of Compton recoil electrons. The sharp drop at the maximum recoil energy is known as the *Compton edge*

$0 < T < T_{\max}$ , where  $T_{\max}$  is the max allowed recoil energy:

$$T_{\max} = h\nu \frac{2\xi}{1 + 2\xi}, \quad \xi = \frac{h\nu}{m_e} \quad (14)$$

### 2.4.3 Pair production

- $\gamma \rightarrow e^- e^+$
- Mean free path:  $\lambda_{\text{pair}} = \frac{9}{7} L_{\text{rad}}$ , where  $L_{\text{rad}} \sim \mathcal{O}(10)$  cm is for electrons

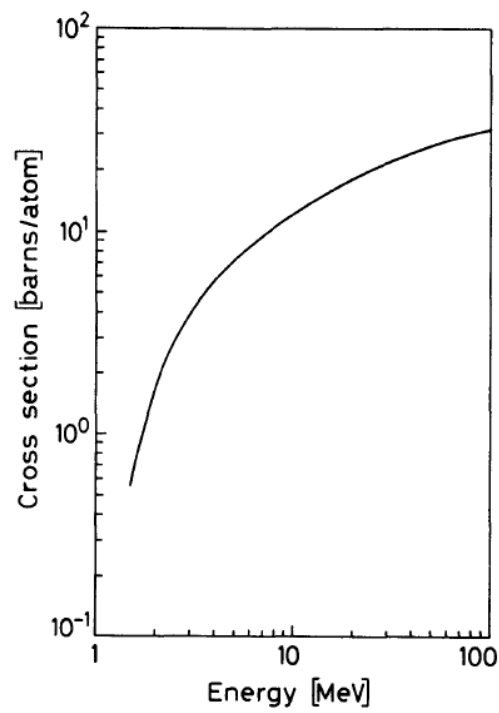


**Fig. 2.25.** Pair production cross section in lead

### 2.4.4 Photon interaction summary

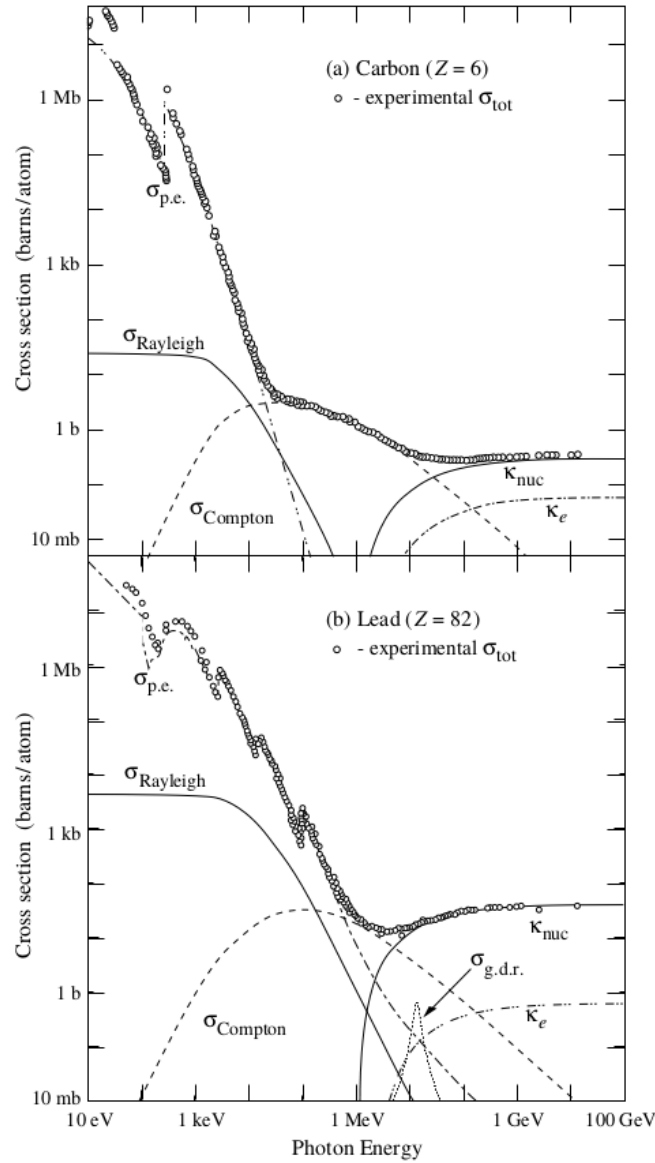


**Figure 32.15:** Photon total cross sections as a function of energy in carbon and lead, showing the contributions of different processes [51]:

$\sigma_{\text{p.e.}}$  = Atomic photoelectric effect (electron ejection, photon absorption)

$\sigma_{\text{Rayleigh}}$  = Rayleigh (coherent) scattering—atom neither ionized nor excited

$\sigma_{\text{Compton}}$  = Incoherent scattering (Compton scattering off an electron)

$\kappa_{\text{nuc}}$  = Pair production, nuclear field

$\kappa_e$  = Pair production, electron field

$\sigma_{\text{g.d.r.}}$  = Photonuclear interactions, most notably the Giant Dipole Resonance [52].

In these interactions, the target nucleus is broken up.

Original figures through the courtesy of John H. Hubbell (NIST).

### 2.4.5 EM showers

- $\gamma \rightarrow e^-e^+, e^\pm \rightarrow e^\pm + \gamma, \gamma \rightarrow e^-e^+ \dots$

- Assuming the radiation lengths are  $L_\gamma \sim L_e$ :
  - $N_{\text{particles}} \sim 2^{x/L}$
  - $E(x) \sim E_0/2^{x/L}$ , where  $E$  is the energy per particle in the shower at distance  $x$
  - Obviously has to truncate when  $E(x) \leq m_e$ , but actually stops at  $E < E_c$  (no more brems)
  - Let  $t = x/L$ . Then,  $t_{\text{max}} = \ln(E_0/E_c)/\ln 2$  and  $N_{\text{max}} \approx E_0/E_c$ 
    - \* Need to add correction for particle that induces shower:  $t_{\text{max}} = \log_2(E_0/E_c) - C$
    - \*  $C = 0.5$  if  $\gamma$ , else  $C = 1$
- Define the Molière radius as the radius of the cylinder surrounding the primary particle that contains 90% of the energy deposited by an EM shower. It satisfies:

$$R_M = X_0 \frac{21.2 \text{ MeV}}{E_c} \quad (15)$$

## 2.5 Interactions of neutrons in matter

- High energy neutrons:  $E > 100 \text{ MeV}$
- Fast:  $\mathcal{O}(100) \text{ keV} < E < \mathcal{O}(10) \text{ MeV}$
- Epithermal:  $\mathcal{O}(0.1) \text{ eV} < E < \mathcal{O}(100) \text{ keV}$  (where nuclear resonances occur)
- Thermal:  $E \sim 1/kT \approx 1/40 \text{ eV}$
- Ultracold:  $E < 0.001 \text{ eV}$

### 2.5.1 Mechanisms of interaction

- $A + n \rightarrow A + n$ : dominant for MeV neutrons (elastic)
- $A + n \rightarrow A^* + n'$ ,  $A + n \rightarrow B + 2n', \dots$ 
  - Neutron must be  $> 1 \text{ MeV}$  to excite the nucleus
  - Inelastic
- Radiative  $n$  capture:  $n + (Z, A) \rightarrow \gamma + (Z, A + 1)$ 
  - $\sigma \sim 1/v$ , so dominant at low energies
  - There can be resonance peaks
- $A + n \rightarrow B + p/d/\alpha/t/\alpha p/\dots$ 
  - Typically eV – keV
  - $\sigma \sim 1/v$
- Fission (more likely at low [thermal] energies)
- High energy hadron shower
  - Similar to EM shower
  - $E > 100 \text{ MeV}$



### 2.5.2 Neutron moderation

- Neutrons bounce around matter, slowing down until at thermal eq. w/ matter
  - Unlikely to be captured by nucleus (or cause fission) at high energies because  $\sigma \sim 1/v$  for these processes
- Energy of scattered neutron:

$$\left(\frac{A-1}{A+1}\right)^2 E_0 < E' < E_0 \quad (16)$$

which implies low  $A$  is better for absorbing energy

## 3 General characteristics of detectors

- Sensitivity to signal is a function of many things:
  - $\sigma$  of ionizing reactions in the detector
  - Detector mass
  - Material surrounding sensitive volume of detector
- Two continuous responses are considered resolved if separated by a distance greater than the FWHM
- Error is Poissonian for detectors that collect *some* of the particle's energy
  - Error is smaller for detectors that *stop* the particle, since each interaction is not independent
- Define  $J = E/W$ , so the energy variance is  $\sigma^2 = FJ$ 
  - $W$  = energy lost per ionization in detector
  - $F$  = Fano factor
    - \*  $F = 1 \Rightarrow$  purely Poissonian (e.g. scintillators in which only part of the energy is deposited)
    - \*  $F < 1 \Rightarrow$  better (semiconductors, gases, scintillators which stop the particle)
  - Resolution can be defined two ways:
    - \*  $\text{FWHM} = 2.35 \frac{\sigma}{J} = 2.35 \sqrt{\frac{FW}{E}}$
    - \* Deviation divided by mean:  $\frac{\sigma}{\mu} = \frac{\sigma}{J} = \sqrt{\frac{FW}{E}}$

## 4 Ionization detectors

### 4.1 Types of gaseous ionization detectors

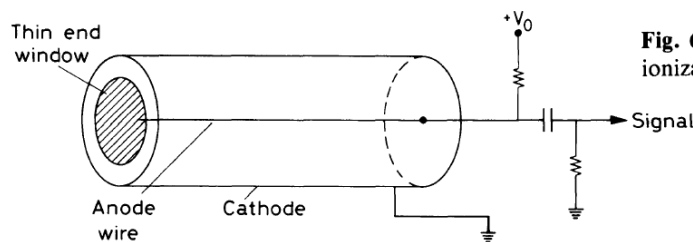


**Fig. 6.1.** Basic construction of a simple gas ionization detector

- Filled with a noble gas

- Radial  $\vec{E}$ -field from anode wire to cathode ( $\propto 1/\ln(b/a)$ , where  $a$  is the wire radius and  $b$  is the chamber radius)
- Radiation creates  $e^-$ /ion pairs in tube
  - If the radiation is charged, this occurs through ionization
  - If neutral, it occurs through secondary ionization (i.e.,  $\gamma, n$  ejects an  $e^-$  from an atom, which then ionizes the gas)
  - Number of pairs is  $\propto E$
  - $e^- \rightarrow$  anode, ions  $\rightarrow$  cathode
  - Observed signal is a function of  $V_0$ :

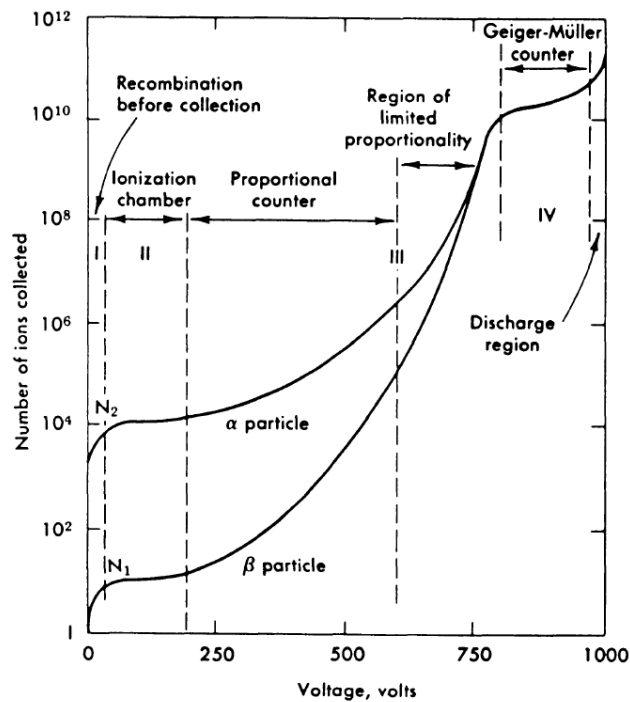


**Fig. 6.2.** Number of ions collected versus applied voltage in a single wire gas chamber (from Melissinos [6.1])

#### 4.1.1 Resistive plate chamber

- Two resistive plates with small gas gap ( $\sim 2$  mm) and large voltage on electrodes outside of the plates ( $\sim 10$  kV)
- Advantage: good time resolution  $\sim 50 - 100$  ps
- Disadvantage: bad signal quality, dark rates

#### 4.1.2 Ionization chamber

- Number of  $e^-$ /ion pairs produced is equal to number of ionizations by particle
- Current is typically quite low
- Can be used for experiments with large radiation fluxes

### 4.1.3 Proportional counter

- $e^-$  from primary ionization drifts towards anode ( $v \sim \mu\text{m/ns}$ )
- $\vec{E}$ -field is strong enough close to the anode that  $e^-$ s from ionization are accelerated and cause secondary ionizations
- These secondary ionization  $e^-$ s can also create tertiary ionizations, and so forth
- Occurs in the “avalanche region” close to the anode (since  $|\vec{E}(r)| \propto 1/\ln(r/a)$ ), typically  $r - a \lesssim 10 \mu\text{m}$
- Up to  $10^6$  amplification

### 4.1.4 Geiger-Müller counter

- $\Delta V$  is so high that an ionization sparks multiple avalanches along entire length of anode
  - $e^-$ s from primary ionization are accelerated so strongly that when they hit an atom, they ionize it but also put the atom in an excited state
  - When the atom de-excites, it releases a  $\gamma$ , which initiates its own avalanche
  - Output current is independent of  $E$
  - Need a quenching gas to absorb  $\gamma$ s and shorten the signal pulse
- Obviously only useful for counting number of incident particles
- If  $V_0 > 1 \text{ kV}$ , you get spontaneous breakdown of the gas, and it is no longer useful

## 4.2 Ionization and transport in gas

- Ionization mechanisms (assuming  $\psi$  is some charged particle):
  - $\psi + X \rightarrow \psi + X^*$  is a resonant process
    - \* In noble gases,  $\sigma \sim 10^7 \text{ b}$
  - $\psi + X \rightarrow \psi + X^+ + e^-$  is not resonant
    - \*  $\sigma \sim 10^8 \text{ b}$
    - \* Higher energy threshold than excitations (need to overcome valence binding energy)
- In general,  $\sigma$  is higher for low-energy transfers, so excitations dominate ionizations
- $e^-$ /ion pairs produced by  $\psi$  can also create secondary  $e^-$ /ion pairs if energetic enough
  - Process repeats until  $E_{e^-} < \text{ionization threshold}$

### 4.2.1 Mean number of $e^-$ /ion pairs

- Note that the number of pairs is not equal to (energy lost)/(ionization energy), because some energy is lost through excitation of atoms
- In noble gases, 1  $e^-$ /ion pair produced corresponds to  $\sim 30 \text{ eV}$  energy lost
- For gaseous detectors, the Fano factor is typically  $\sim 0.2$

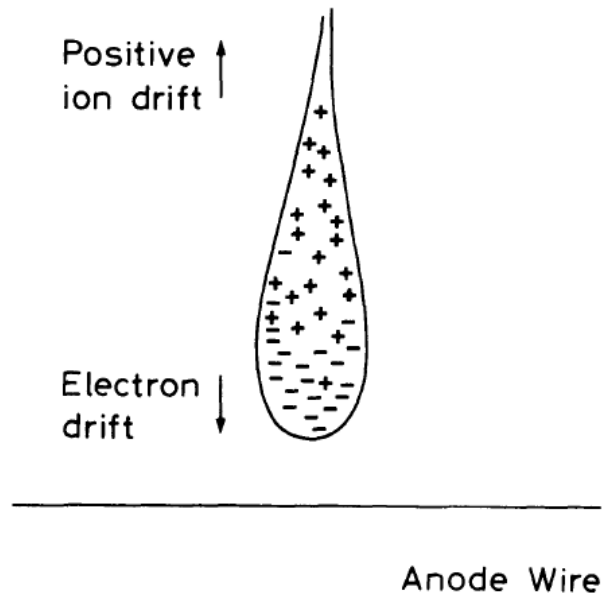
### 4.2.2 Recombination and $e^-$ -attachment

- These processes eat up  $e^-$ /ion pairs before detection
- Recombination: if  $\psi + X \rightarrow \psi + X^+ + e^-$ , then we can have  $X^+ + e^- \rightarrow X + \gamma$ 
  - Similarly, if two ions exist in the gas:  $X^+ + Y^- \rightarrow XY + \gamma$
- Electron attachment: capture by electronegative atoms:  $e^- + Y \rightarrow Y^- + \gamma$

### 4.2.3 Diffusion

- In principle, a charged particle in a detector will follow the  $\vec{E}$ -field lines
- But, it can be knocked about through elastic collisions with atoms
- Problem for detectors in which electrons must drift very far
- One way to minimize the effect is to add a parallel  $\vec{B}$ -field (so that if a particle is knocked off the field line, it remains in a tight helix). This is done in TPCs

## 4.3 Avalanche multiplication



- The initial  $e^-$  has high energy and causes secondary, tertiary, etc ionizations
- $e^-$ s move much faster than ions, giving the charge distribution a liquid drop shape
- Let  $\lambda$  be the mean free path of an  $e^-$  causing secondary ionization
  - $\alpha = \lambda^{-1}$  is the prob. of ionization/unit length

$$dn = n\alpha dx \quad (17)$$

where  $n$  is the number of free  $e^-$ . Then:

$$n = n_0 e^{\alpha x} \quad (18)$$

where  $n_0$  is the number of primary ionizations

- $e^{\alpha x}$  is the proportionality factor in prop. counters
- Above calculation assumes a constant  $\vec{E}$ -field  $\Rightarrow$  constant  $\alpha$ 
  - More generally:

$$e^{\alpha x} \rightarrow \exp \left[ \int_{r_1}^{r_2} dx \alpha(x) \right] \quad (19)$$

#### 4.4 Pulse formation and shape

- Consider a cylindrical proportional counter as an example
- Consider the counter as a coax capacitor with capacitance/unit length  $C$ 
  - If a charge  $q$  moves by  $dr$ , then

$$dW = q \frac{d\phi}{dr} dr \quad (20)$$

where  $W$  is the system energy and  $\phi$  is the electric potential

- For a capacitor of length  $L$ ,  $W = \frac{1}{2} L C V_0^2$ , so

$$dW = L C V_0 dV \quad (21)$$

- Equating:

$$dV = \frac{q}{L C V_0} \phi'(r) dr \quad (22)$$

- That is, the motion of  $q$  by  $dr$  induces a measurable change in the potential

- $\Rightarrow$  observed signal is *not* charges collecting on the wire/wall, but an induced voltage change due to moving charges
- The total induced voltage change for a particle starting a distance  $r'$  from the wire is:

$$\int dV = \int_{a+r'}^R dr \frac{q}{L C V_0} \phi'(r) \quad (23)$$

where  $R = a$  ( $R = b$ ) for  $e^-$  (ions).

- Avalanches only occur when the  $\vec{E}$ -field is very high (close to the anode), so typically  $r \sim \mathcal{O}(1) \mu\text{m}$  ( $a \sim \mu\text{m}$ ,  $b \sim \text{mm}$ )
- i.e.  $b - (a + r') \gg r' \Rightarrow$  pulse is primarily caused by motion of positive charges
- For many (but not all!) types of prop. counters, can ignore signal from  $e^-$
- In the following figure, time starts with the beginning of the avalanche (drift time is ignored)

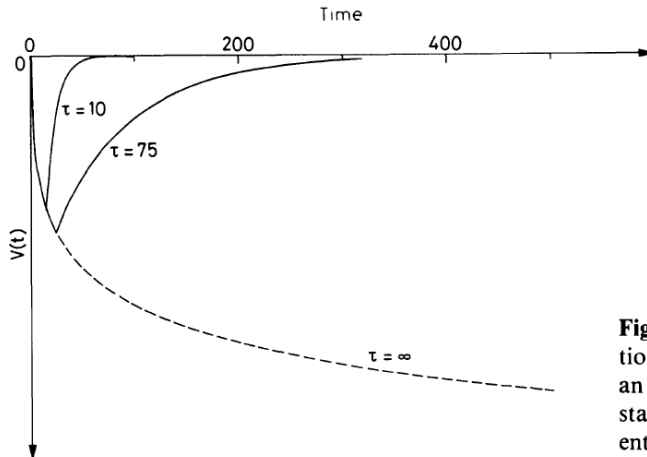
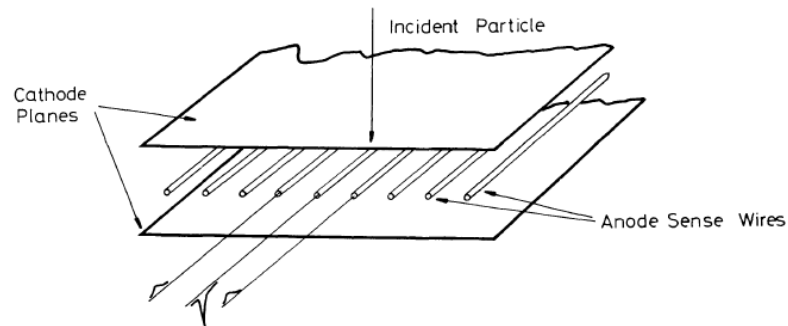


**Fig. 6.6.** Pulse signal from a cylindrical proportional counter. The pulse is usually cut short by an  $RC$  differentiating circuit with a time constant  $\tau$ . The figure shows the effect of two different constants

## 4.5 Multiwire proportional chamber

**Fig. 6.7.** Basic configuration of a multiwire proportional chamber. Each wire acts as an independent proportional counter. The signal on the firing wire is negative while the signals on the neighboring wires are small and positive



- Cathode planes are separated by  $\sim 10$  mm and the wires are spaced  $\sim 2$  mm apart
  - Spatial resolution is  $\sim 1/2$  of wire spacing
- The efficiency of a particle creating a signal is typically  $\sim 99\%$
- Free  $e^-$ /ions drift towards nearest wire/cathode wall
- Upon getting close to the anode,  $e^-$  can induce avalanche
- Ions from avalanche induce negative voltage difference on anode (same as proportional counter)
- Also induces a small *positive* signal on adjacent anodes
- Can align many MWPCs (with alternating layers at right angles) to determine trajectory
  - With sufficiently many such layers, can get 3D particle trajectory reconstruction

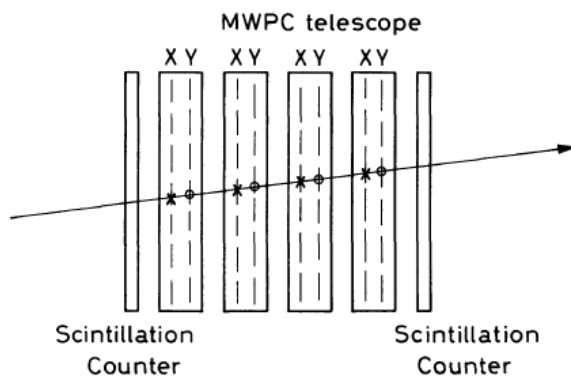


**Fig. 6.9.** A MWPC telescope for particle tracking. Each MWPC contains an  $X$  and  $Y$  wire plane. If the MWPC's are aligned, the measured coordinates allow a reconstruction of the particle trajectory. More than two planes of wires in a chamber may also be used

- Since each anode wire is a separate detector, MWPCs can detect multiple particles, as long as they do not overlap
- Magic gas: 75% Ar, 24.5% isobutane, .5% freon  $\Rightarrow$  gains up to  $\sim 10^7$ 
  - Argon is used because noble gases require smallest  $\vec{E}$ -field for avalanche
  - Above gains of  $\sim 10^3$ , argon atoms will become excited and then de-excite by releasing a  $\gamma \Rightarrow$  can release photoelectric  $e^-$  in cathode
  - Add a quenching gas (isobutane) to absorb  $\gamma$ s and dissipate energy thermally

- Freon is added to kill any remaining dark current (i.e. electrons escaping from cathode due to high  $\vec{E}$ -field). Freon is very electronegative and therefore can capture low-energy  $e^-$ s
- If magic gas is used:
  - The signals are saturated and independent of energy  $\Rightarrow$  can be used for position tracking
  - High gain  $\Rightarrow$  signal from  $e^-$ s is measurable. This is much faster than the ion signal, giving better timing resolution  $\sim 25\text{-}30$  ns
- Multiple firings

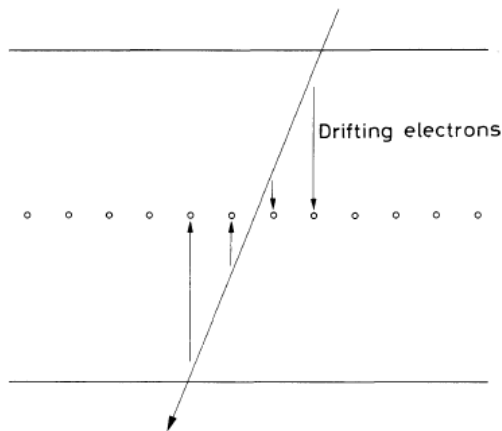


**Fig. 6.13.** Track clusters caused by particles arriving at an angle to the anode plane

- The first and last ionizations in the diagram above will give delayed signals (wrt the second and third ionizations) because of the  $e^-$  drift time
- Typically use this timing info to get the signal localized to one or two anode wires

#### 4.6 Drift chamber

- Similar to proportional counter. Uses many “field wires” held at constant potential to ensure uniform  $\vec{E}$ -field
- Uniform  $\vec{E}$ -field  $\Rightarrow$  constant drift velocity

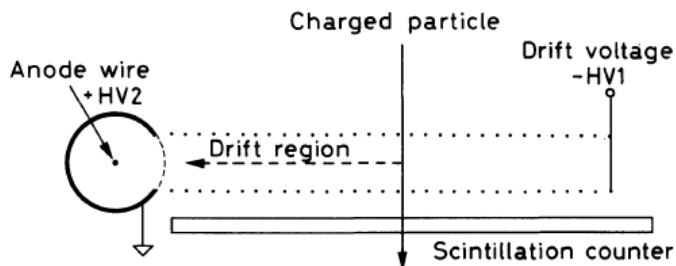


**Fig. 6.15.** Basic operating principle of the drift chamber (from Sauli [6.3])

- Operation:
  - Particle sets off scintillator. Timer starts
  - Particle ionizes an atom in chamber.  $e^-$  drifts to anode
  - $e^-$  reaches (near) anode, inducing a signal through avalanche. Timer stops
  - Using  $\Delta t$  and constant drift velocity of  $e^-$ , position in  $z$  can be determined

- Spatial resolution is now determined by timing resolution of scintillator and anode signal
  - $\Rightarrow$  no longer need high wire density (like MWPCs)
- Max counting rate is  $\sim 10^4/(\text{s}\cdot\text{mm})/\text{wire}$ 
  - Same as MWPCs, but fewer wires  $\Rightarrow$  smaller flux can be handled

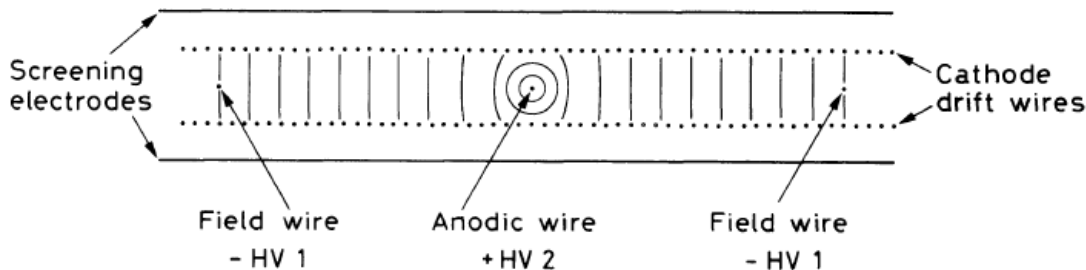


**Fig. 6.16.** Drift chamber design using interanode field wires (from *Breskin et al.* [6.22])

- Cylindrical drift chambers used at collider detectors
- Drift chamber is much more sensitive to gas composition, pressure, impurities, because all these things affect constant drift velocity assumption
- Correction needs to be made to account for presence of a  $\vec{B}$ -field
- Drift velocity of  $e^-$  is  $\sim \mathcal{O}(10) \mu\text{m}/\text{ns}$  in Ar
- Higher drift velocity  $\Rightarrow$  lower uncertainty from diffusion

## 4.7 Time projection chamber

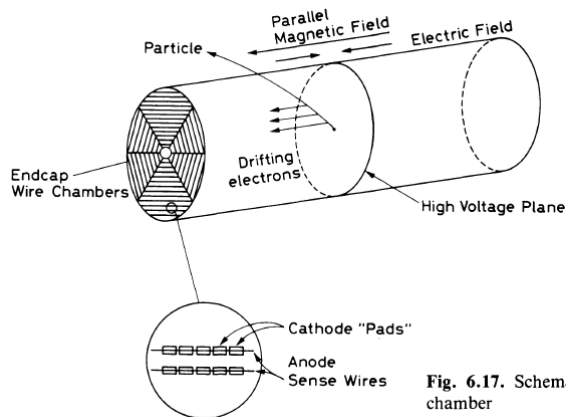
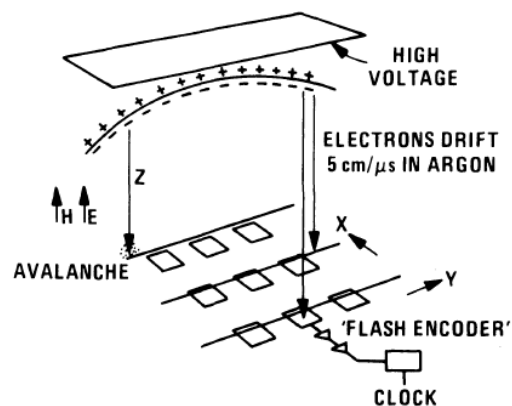


**Fig. 6.17.** Schematic diagram of a time projection chamber



- Combines principles of a MWPC and drift tube, as well as giving info on particle momentum and  $dE/dx$
- Constant  $\vec{E}$ -field  $\Rightarrow$  electron drift velocity is constant
- $\vec{B}$ -field has two purposes:
  - Curves tracks of charged particles
  - Ensures  $e^-$  diffusion (multiple scattering) is always helical towards endcap of TPC



- 3D reconstruction:
  - 1D from which anode wire gets a signal
  - 1D from which cathode pads get charge on them
  - 1D from drift time
- Typically add a grid held at ground potential right before endcap
  - Traps positive ions before they drift back to central cathode
- Charge/signal on cathode pads/anode wires is  $\propto$  energy of drift  $e^- \Rightarrow$  gives  $dE/dx$  of particle
- Curvature of charged particle gives the momentum
- Anode wire spacing is  $\sim 1$  cm
- Scintillation (i.e. for LAr TPC)
  - Liquid argon better for number of reasons
    - \* Higher density than gas (good for low  $\sigma$  interactions like  $\nu N$ )
    - \* Scintillator
    - \* Very low electronegativity
  - If the gas (or liquid) is a scintillator, can add photodetectors to measure position along  $z$  axis
  - Can use this info to know where the ionization occurred (instead of relying on drift time)

## 5 Scintillators

- Particle excites an atom/molecule, which then de-excites by releasing a  $\gamma$
- Emitted light is picked up by a photodetector
- Features
  - Above energy threshold, scintillator response is  $N_\gamma \propto E$ . Since photomultipliers have  $N_e \propto N_\gamma$ , the total response is linear in  $E$
  - Very short deadtime, very fast response
  - Can distinguish particle type based on pulse shape
- If  $N(t)$  is the number of photons emitted at time  $t$ , it can be approximated as the sum of a fast and slow components:

$$N = A \exp \left[ -\frac{t}{\tau_f} \right] + B \exp \left[ -\frac{t}{\tau_s} \right] \quad (24)$$

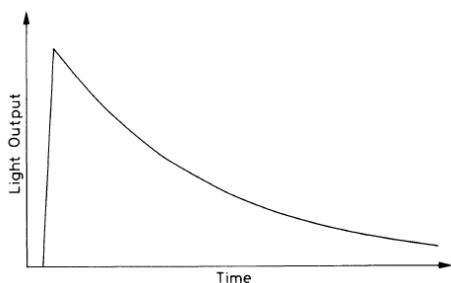


Fig. 7.2. Simple exponential decay of fluorescent radiation. The rise time is usually much faster than the decay time

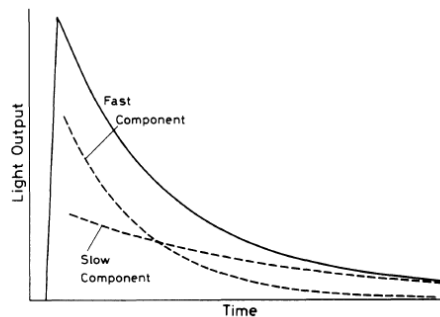


Fig. 7.3. Resolving scintillation light into *fast* (prompt) and *slow* (delayed) components. The *solid line* represents the total light decay curve

The values of  $A$  and  $B$  depend on the material and particle type (can be used for particle ID)

- Note that the above formula ignores the rise time (typically very short relative to the decay, so can be ignored).
- Desirable features:
  - High efficiency from energy lost to radiation
  - Transparency to radiation (so it can reach PMTs)
  - Emission range is in operating range of PMT
  - Short decay time  $\tau$
- Scintillators can be used as liquids or solids
- Liquid scintillators can be *loaded* with other things for specific purposes (e.g. Gd or B for high neutron capture  $\sigma$ )
- Energy loss ranges from 20 to 500 eV/photon

## 5.1 Organic scintillators

- Response time:  $\leq$  few ns
- Molecules get excited
- Can have singlet ( $S_0$ ) or triplet ( $T_0$ ) spin ground state

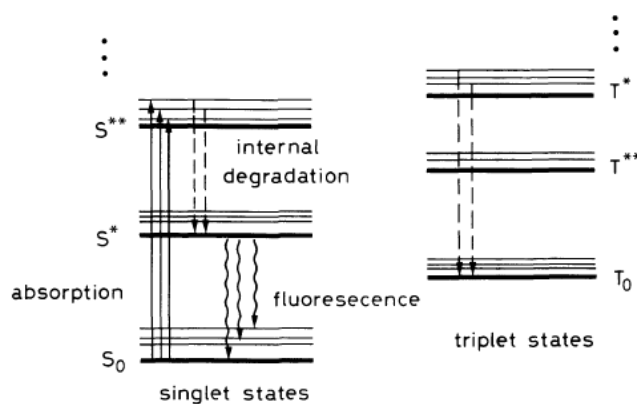


**Fig. 7.4.** Energy level diagram of an organic scintillator molecule. For clarity, the singlet states (denoted by  $S$ ) are separated from the triplet states (denoted by  $T$ )

- $S^*$  and  $S^{**}$  are electron excitations
- Excitation mechanism:
  1. Excitation goes from  $S_0$  to  $S^{**}$  (or one of its vibrational excitations).
  2. Then, internal degradation to  $S^*$  (no  $\gamma$  released)
  3. Then, fluorescence to vibrational excitation of  $S_0$  (or  $S_0$  itself)
  4. Since bulk of atoms are in  $S_0$ , photons from de-excitation to vibrational excitation of  $S_0$  will not be re-absorbed
- Similar story for triplet states, but  $T_0 \rightarrow S_0$  is suppressed. Instead have  $T_0 + T_0 \rightarrow S^* + S_0 + \text{phonons}$
- Liquids have a response time of  $\tau \sim 3 - 4$  ns

- Plastics
  - Organic apparently
  - Very fast response  $\Rightarrow$  rise time cannot be ignored
  - $\tau \sim 2 - 3$  ns

## 5.2 Inorganic crystals

- Much slower  $\tau \sim 500$  ns
- Main advantage is high stopping power because of high density and  $Z$
- Higher light response ( $2-10\times$ ) than organics
  - $\Rightarrow$  better energy resolution
  - Useful for high energy  $\gamma$  or  $e^\pm$
- Ex: NaI or  $\text{PbWO}_4$
- Scintillation mechanism:
  - $e^-$  can be excited from valence band to excitation or conduction bands
  - If excitation band, the  $e^-$ -hole pair is in a bound state (exciton) that moves through the crystal
  - If the exciton hits an impurity, the  $e^-$  is absorbed by the impurity  $\Rightarrow$  just a hole left behind
  - Then, an  $e^-$  passing by (from a higher energy state than the hole) will fill the hole, radiating a  $\gamma$

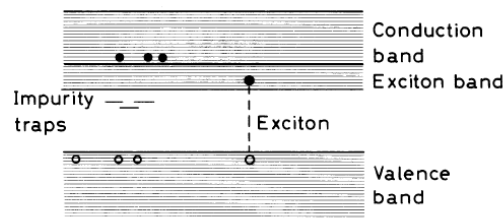


**Fig. 7.7.** Electronic band structure of inorganic crystals. Besides the formation of free electrons and holes, loosely coupled electron-hole pairs known as excitons are formed. Excitons can migrate through the crystal and be captured by impurity centers

## 5.3 Gas

- Very fast  $\tau \sim 1$  ns
- Emits in UV range

## 5.4 Pulse shape discrimination for particle ID

- Fast and slow components of decay depend on  $dE/dx$
- The components correspond to different de-excitations with different  $\Delta E$  wrt ground state
  - Which excitations are populated is therefore dependent on  $dE/dx$

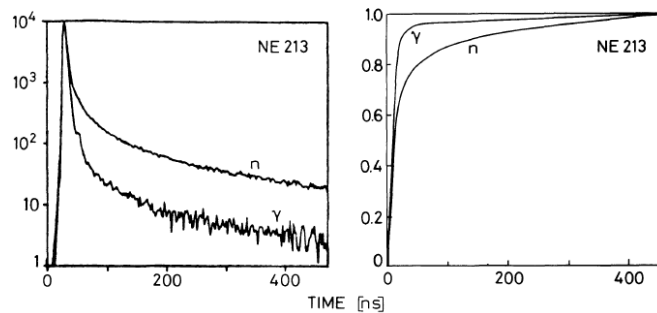


**Fig. 7.12.** Pulse shape differences of NE213 liquid scintillator light for neutrons and gamma rays. The time integral of the light pulses is also shown. A discrimination between these radiations may be obtained by measuring the time it takes for the integrated pulse to reach a certain fixed level (from *Lynch* [7.17]; picture © 1975 IEEE)

## 5.5 Quenching

- Energy lost through de-excitations that do not radiate a  $\gamma$ 
  - e.g. through phonons or if the atom is ionized and the  $e^-$  is recaptured later
- Issue for heavy ions and  $\alpha$ s, which heavily ionize
  - Inorganic scintillators used in this case, as they have a higher light output
- Quenching  $\Rightarrow$  lower light output

## 5.6 Electron detection

- “Efficiency” close to 100%
- *However* if scintillator is high  $Z$ , may backscatter out of detector before depositing full energy
  - The 100% therefore refers to particles being counted, not energy measurement
- For low-to-medium  $e^\pm$  energies, use low  $Z$  organic scintillators
- High  $Z$  inorganics good at high energy (facilitates EM shower production, depositing full energy)

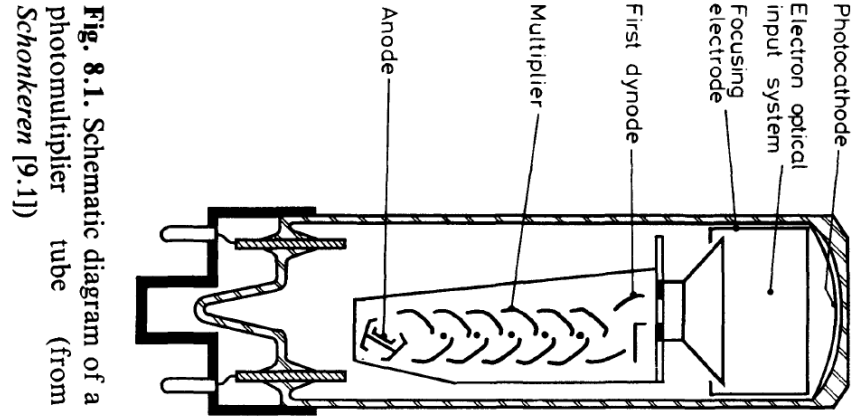
## 5.7 Photon detection

- Want photoelectric and pair production ( $\gamma$  absorbed) to dominate Compton ( $\gamma$  scattered)
- $\sigma_{\text{photo}} \propto Z^5$ ,  $\sigma_{\text{pair}} \propto Z^2$ ,  $\sigma_{\text{Compton}} \propto Z$
- $\Rightarrow$  high  $Z$  is better for  $\gamma$ s

## 5.8 Neutron detection

- High energy: look for recoil in  $A + n \rightarrow B + p$ 
  - Organics good for this
  - Pulse shape to reject  $\gamma$ -backgrounds
- Thermal: use  $A + n \rightarrow B + \gamma/\alpha$ 
  - Use things that have neutron capture  $\sigma$ : Li, B, Gd

## 6 Photomultipliers



- Operation principle:
  1.  $\gamma$  hits cathode, ejects  $e^-$  through photoelectric effect
  2.  $e^-$  is accelerated to first dynode, where it knocks out multiple  $e^-$  s
  3. These are accelerated to the next dynode, each knocking out multiple  $e^-$  s, and so on
  4. Number of electrons reaching anode is roughly constant per photon
- Photon must typically be in narrow energy range (i.e. from scintillator)

### 6.1 Photocathode

- Quantum efficiency:

$$n(\lambda) = \frac{\# \text{ of photoelectrons released}}{\# \text{ of incident photons with wavelength } \lambda} \quad (25)$$

- Typically, semiconductors are used instead of metals (higher QE)
  - Suppose an  $e^-$  absorbs a  $\gamma$  and is traveling to the surface of the material
  - If material is metal, many interactions with free  $e^-$  s  $\Rightarrow$  high  $dE/dx$   $\Rightarrow$  energy when it reaches surface may be too low to overcome potential barrier
  - Semiconductor  $e^-$  s are typically in valence bands or tightly bound  $\Rightarrow$  low  $dE/dx$

### 6.2 Multiplier dynodes

- Dynodes are made of insulator coating a conductor
- Typically 10-14 dynodes/tube
- Gains of  $10^6$ - $10^7$

### 6.3 Gain and voltage supply

- Let  $V_d$  be the voltage between adjacent dynodes. The gain in  $N_e^-$  is  $\delta = KV_d$ , for some factor  $K$
- The total gain, given  $N$  dynodes, is  $G = (KV_d)^N$ , assuming the same  $V_d$  for all dynode pairs

## 6.4 Pulse shape

- We assume the input photon distribution is from a scintillator with exponentially decaying response
- Then, the current is also exponentially decaying:  $I = dQ/dt$ ,  $Q = N_e \propto N_\gamma$

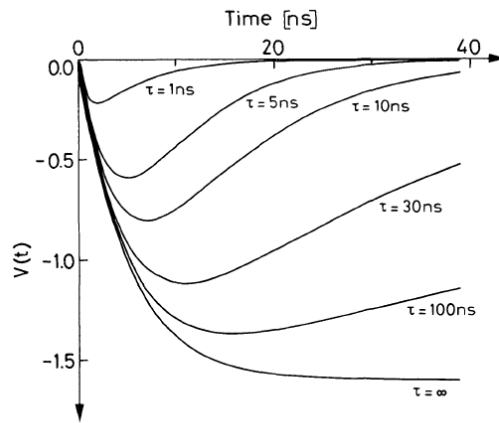


**Fig. 8.13.** Output signals for various time constants  $\tau$  (after Wright [8.8])

## 6.5 Time resolution and response

### 6.5.1 Geometry of PMT

- Electrons from different parts of the cathode take different amounts of time to reach first dynode
- Spread in transit time is  $\Delta t \sim 0.5$  ns. The transit time itself is  $\sim 0.2$ - $0.5$  ns
- Above values are reached by using non-uniform  $\vec{E}$ -field between cathode and first dynode

### 6.5.2 Noise

- Dark current and after pulsing
  - DC is mostly from thermal noise
  - DC is exponential in  $-\phi$  (work function); materials with  $\phi < 0$  (good for PE effect) have high DC
  - Two sources of after pulses:
    - \*  $\gamma$  released from dynode when  $e^-$  hits. It can go back and release another  $e^-$  from the cathode
    - \* Ions created when  $e^-$  travelling through tube hits residual gas molecules. Ion travels back to cathode, release  $e^-$
- Statistical noise
  - Due to statistical nature of PE effect
  - Fluctuations in the electron multiplier system
    - \* Statistical fluctuations in secondary emission
    - \* Difference in  $e^-$  transit times between dynodes

## 7 Semiconductor detectors

### 7.1 Basic principles

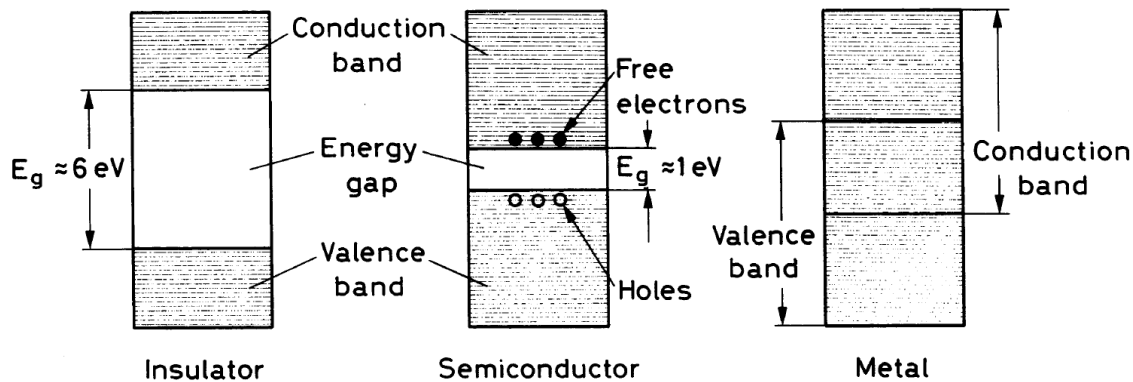


**Fig. 10.1.** Energy band structure of conductors, insulators and semiconductors

- Energy “bands” are actually many close, discrete energy levels  $\Rightarrow$  treat them as continuous
  - Arise from degenerate lattice energy levels breaking into many close discrete levels (due to Pauli principle)
- Below the valence band are tightly-bound  $e^-$  s
- Conduction band: free to roam in lattice
- Valence band: more tightly bound to individual atoms
- In an insulator, the bands are far apart. In a semiconductor, the band gap is  $\sim 1 \text{ eV}$
- When a voltage is applied:
  - Insulator: valence  $e^-$  s are stuck  $\Rightarrow$  no current
  - Metal: Thermally excited  $e^-$  s are in the conduction band  $\Rightarrow$  current flows
  - Semiconductor: only a few  $e^-$  s in the conduction band, so a small current is observed. As  $T \rightarrow 0$ , the current decreases
- Charge carriers in semiconductors
  - Thermal excitation:  $e^-$  jumps to conduction band, leaving hole behind
    - \* Conduction band  $e^-$  can move freely  $\Rightarrow$  one current
    - \* Valence band can also move freely  $\Rightarrow$  another source of current
    - \* Hole current is due to  $e^-$  s moving around to fill holes
    - \* In contrast, metals only have one type of current (free  $e^-$ )
  - Number of  $e^-$ /hole pairs is  $\propto T^{3/2} \exp[-E_g/2kT]$ , where  $E_g$  is the energy gap size at 0 K
- Recombination
  - Process of  $e^- + \text{hole} \rightarrow \text{phonon}$
  - Expect  $e^-$ /hole lifetime  $\sim 1 \text{ s}$ 
    - \* Long because in order for recombination to occur,  $e^-$  and hole must be in specific energy/momentum configuration
  - Experimentally, find  $\tau \sim 1 \mu\text{s} - 100 \mu\text{s}$   $\Rightarrow$  some other mechanism of destroying pairs

- Impurities can add energy levels in the energy gap

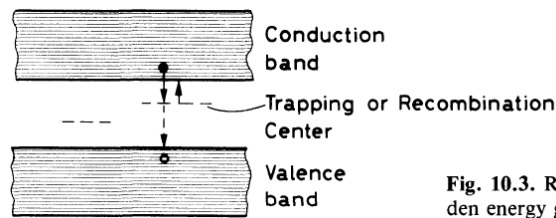


**Fig. 10.3.** Recombination and trapping sites in the forbidden energy gap

- \* These intermediate states can capture an  $e^-$  and later capture a hole (or vice versa), causing recombination
- \* Very efficient process
- \* Bad for detection, as it reduces charge carrier lifetime (i.e. recomb. occurs before the charges can be collected)
- \* Detectors need  $< 10^{10}$  impurities/cm<sup>3</sup>
- Trapping
  - \* Similar to recombination impurities, except the extra energy states are charge-specific (i.e. only  $e^-$  or holes, but not both)
  - \* Charge is then released after some characteristic time
    - If the capture time is longer than charge collection time, signal can be lost to trapping centers
- Recomb. and trapping effects can arise from structural defects in lattice as well

## 7.2 Doped semiconductors

- A semiconductor can be doped when a lattice atom is replaced with an atom with:
  - An extra  $e^-$   $\Rightarrow$  donor (n-type) impurity
  - A missing  $e^-$   $\Rightarrow$  acceptor (p-type) impurity
- For example, if the semiconductor is Si or Ge (quadravalent atoms), a donor would have 5 valence  $e^-$  (e.g. P), and an acceptor would have 3 valence  $e^-$  (e.g. Al)

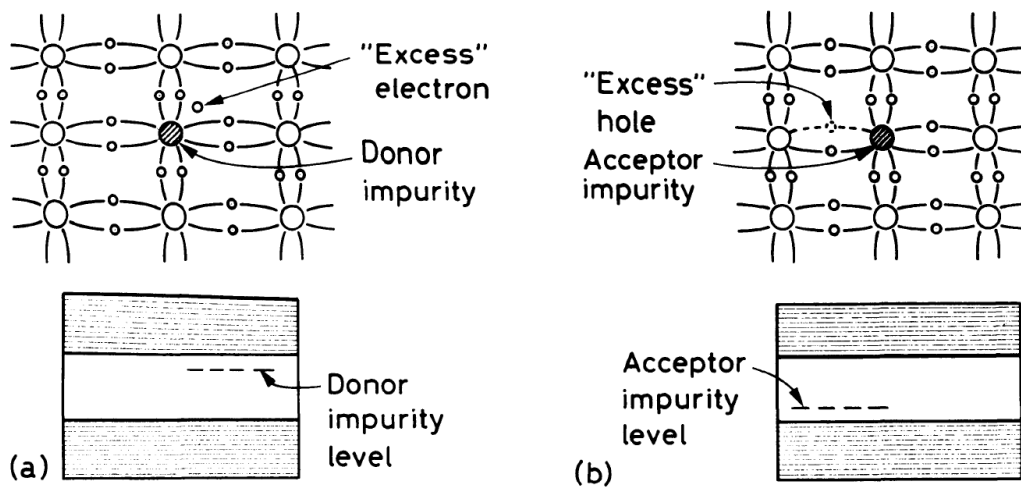


**Fig. 10.4.** (a) Addition of donor impurities to form n-type semiconductor materials. The impurities add excess electrons to the crystal and create donor impurity levels in the energy gap. (b) Addition of acceptor impurities to create p-type material. Acceptor impurities create an excess of holes and impurity levels close to the valence band



- n-type (i.e. extra  $e^-$ )
  - Valence band is filled up, so extra  $e^-$  creates an energy level in the gap
  - The  $\Delta E$  between the impurity state and the conduction band is  $\mathcal{O}(0.01)$  eV
  - This extra  $e^-$  is very easily thermally excited into conduction band  $\Rightarrow$  better conductivity
  - Extra  $e^-$  will also drop down to fill holes  $\Rightarrow$  hole current is somewhat suppressed
- p-type (i.e. missing  $e^-$ )
  - Essentially everything said about n-type, but  $e^- \longleftrightarrow$  hole.
  - Impurity level is very close to valence band (i.e. location of hole current)
- Let  $p, n$  be the concentrations of positive, negative (i.e. holes, free  $e^-$ ) charges respectively;  $N_D, N_A$  be the concentrations of donor, acceptor impurities. Then, electric neutrality implies:

$$N_D + p = N_A + n \quad (26)$$

- Note that donors are positively charged: extra  $e^-$  is not in valence band (so it is counted as part of  $n$ ). Inverse is true for acceptors

### 7.3 The np junction and depletion zone

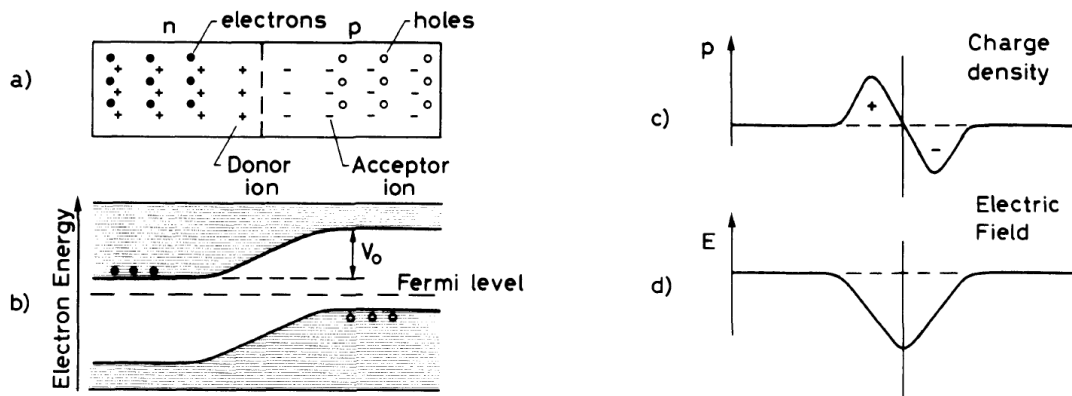


**Fig. 10.5.** (a) Schematic diagram of an np junction, (b) diagram of *electron* energy levels showing creation of a contact potential  $V_0$ , (c) charge density, (d) electric field intensity

- Basic concept: p-type semiconductor next to n-type material (actual fabrication is more complicated)
- n- and p-sides start neutral, but then:
  - $e^-$  flow from n to p, filling holes
  - Holes from p to n, accepting  $e^-$
  - $\Rightarrow$  result: p-side has static negative charge; n-side has static positive charge
  - Static charge distributions are localized near boundary
- Generates an  $\vec{E}$ -field from n to p. **IMPORTANT:** sign of  $\vec{E}$ -field in above diagram (from Leo) is incorrect
- The  $\vec{E}$ -field is equiv to a potential difference across junction ( $V_0 \sim 1$  V)
- Non-zero  $\vec{E}$ -field pushes the energy levels up (down) on the p (n) side
  - Remember:  $e^-$  move against  $\vec{E}$

- More negative static charges on p-side  $\Rightarrow e^-$  energy levels go up
- More positive static charges on n-side  $\Rightarrow e^-$  energy levels go down
- Capacitance: the electrostatic configuration resembles a plate capacitor with  $C \sim \text{pF}/\text{mm}^2$
- Depletion zone
  - Area in which there are no free charges
  - Depth of n- and p-sides (calculation is below):

$$x_n = \sqrt{\frac{2\epsilon V_0}{eN_D(1 + N_D/N_A)}}, \quad x_p = \sqrt{\frac{2\epsilon V_0}{eN_A(1 + N_A/N_D)}} \quad (27)$$

- $\Rightarrow$  if one side is more heavily doped than the other, the depletion zone extends further into the lightly-doped side
- Depth calculation:

Assume the charge density is constant:

$$\rho(x) = \begin{cases} -eN_D & 0 < x < x_n \\ -eN_A & -x_p < x < 0 \end{cases} \quad (28)$$

Charge conservation implies  $x_n N_D = x_p N_A$ . Using Poisson's equation:

$$\phi''(x) = -\rho(x)/\epsilon \quad (29)$$

Integrating twice and choosing constants:

$$\phi(x) = \begin{cases} -\frac{eN_D}{\epsilon} \left( \frac{x^2}{2} - x_n x \right) & x \in n \\ -\frac{eN_A}{\epsilon} \left( \frac{x^2}{2} + x_p x \right) & x \in p \end{cases} \quad (30)$$

Imposing  $\phi(-x_p) = 0$  and  $\phi(x_n) = V_0$  allows us to solve for the depths.

## 7.4 Semiconductors as detectors

- Principle: constant  $\vec{E}$ -field in depletion zone carries away charges from ionization
  - Holes go to p-side
  - $e^-$  go to n-side
- Average energy to create  $e^-$ /hole pair is 3 eV
  - Can contrast with gases  $\sim 30$  eV
  - Scintillators are  $\sim 300$  eV
- For light particles ( $m \lesssim m_p$ ), energy per ionization  $w$  is independent of particle type
  - Therefore, given a collection efficiency  $n$ , particle of energy  $E$ , and assuming the particle is stopped in the semiconductor:

$$Q = \frac{nE}{w} \quad (31)$$

- Not quite true for heavier ions  $\alpha, \dots$
- What is measured is a voltage difference induced by charge collected  $Q \Rightarrow V = Q/C$

### 7.4.1 Reverse bias

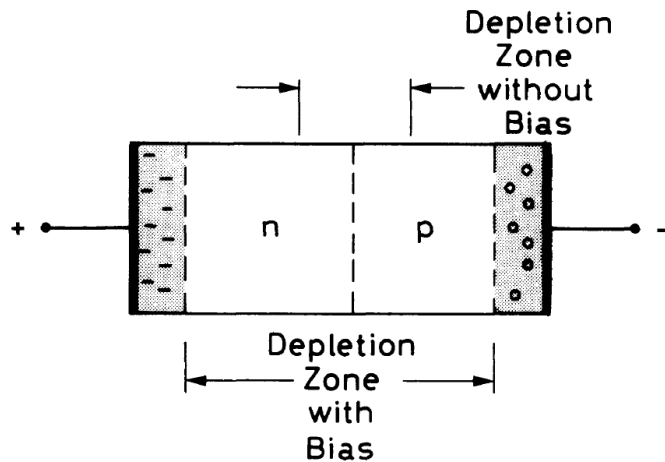


**Fig. 10.7.** Reversed-bias junction

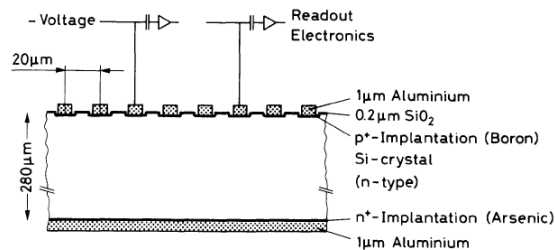
- Normal depletion zone is rather small and  $\vec{E}$ -field is relatively weak
- Fix both issues by adding an additional bias voltage  $V_B \gg V_0$
- Note:  $V_B$  is maintained and  $V_B \gg V_0$ , so changing  $V_0$  due to individual ionizations is negligible
- Can get depletion zones of  $\sim 1$  mm

### 7.4.2 Detector characteristics

- Fano factor is  $\sim 0.12 \Rightarrow$  energy resolution for a 5 MeV particle is  $\sim 0.07\%$
- Response is very fast  $\sim 10$  ns, and timing resolution can get down to  $\sim 10$  ps
  - Drift time is  $\sim 10$  ps/ $\mu\text{m}$  in silicon
- Dimensions are typically  $\sim 100 \mu\text{m} \Rightarrow$  spatial resolution is dimension divided by  $\sqrt{12}$

## 7.5 Silicon strip detectors

- Same basic principle as the detectors described above, just in a different geometry

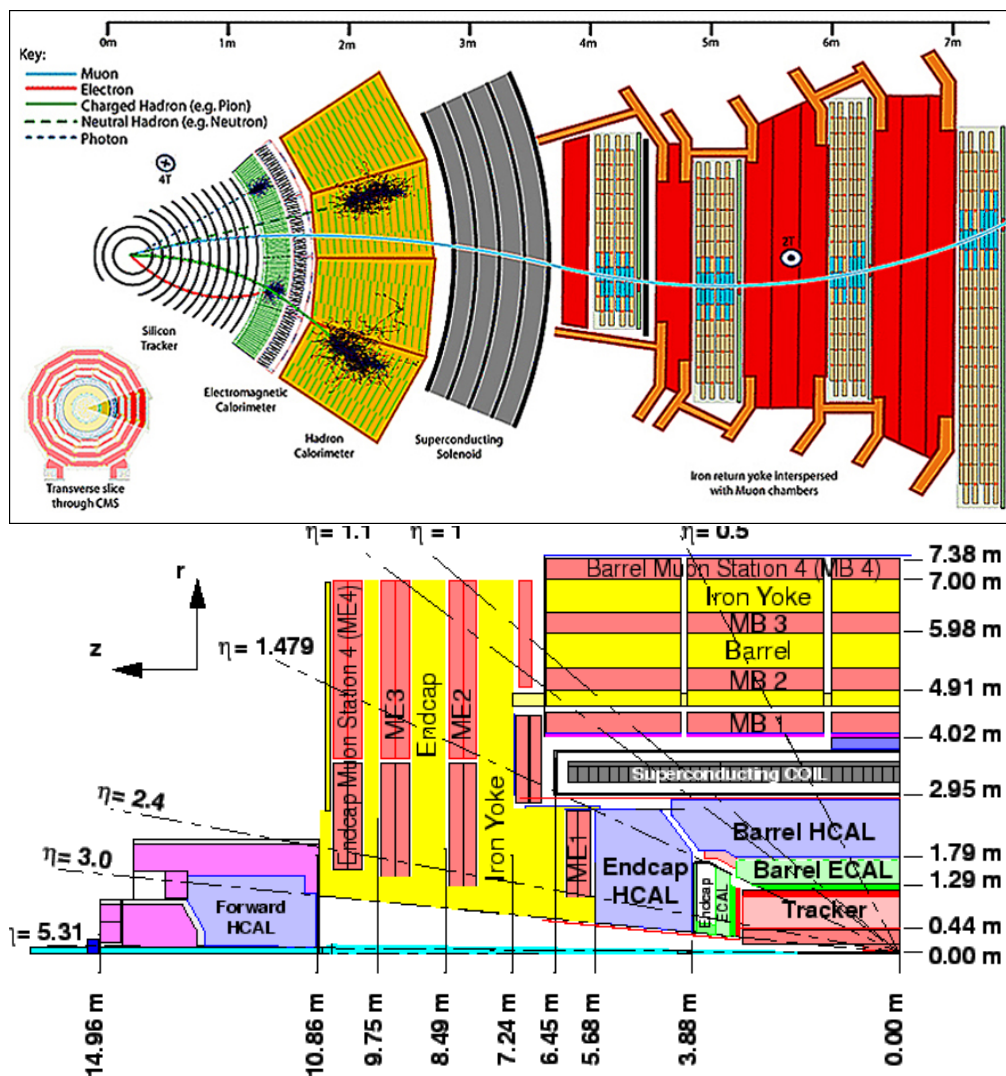


- p-type strips embedded in n-type bulk
- Thickness is typically  $\sim 300 \mu\text{m}$ . Can get much larger depletion zone
- Spatial resolution is better than spacing of strips: can use the amount of charge deposited on each strip to interpolate where the ionization happened
  - $\Rightarrow \sigma \sim 5 \mu\text{m}$  if the spacing is  $20 \mu\text{m}$
  - Typically factor of 3-7 $\times$  improvement

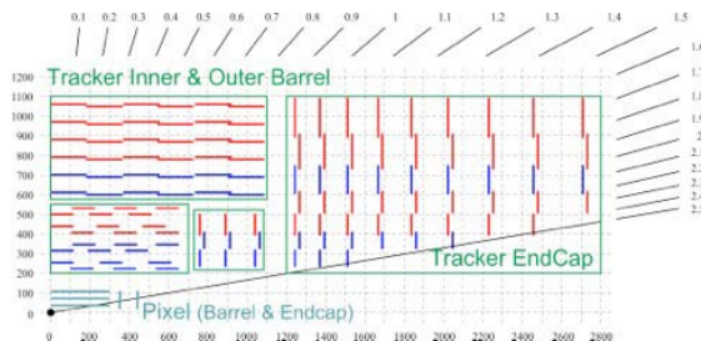
## 7.6 Silicon photomultipliers

- Like with PMTs, the photon hits a semiconductor (such as silicon dioxide) and ejects a photoelectron
- If the bias voltage is large enough, the pair can cause secondary ionizations  $\Rightarrow$  avalanche
- In Geiger mode, can get gains of  $\sim 100$
- CMS ECAL avalanche photodiodes have a total efficiency (quantum times collection) of 70%
- A SiPM is a large array of APDs in Geiger mode
  - Downside is large dark rate

## 8 Compact Muon Solenoid



## 8.1 Silicon tracker



- Reasons to use a silicon tracker:
  - Fine granularity and fast response time
  - Radiation resistant
  - $\sim 1\%$  resolution at  $p_T = 100$  GeV
  - Can measure impact parameter of tracks (i.e. vertexing) very well:  $\sigma_{IP} \sim 20 \mu\text{m}$
- Lorentz drift of charges
  - Drift of charges in detectors is affected by  $\vec{B}$ -field
  - Can lead to charge sharing: multiple pixels set off by a single hit
  - *If reconstructed properly*, can actually improve spatial resolution (i.e. the amount of charge sharing can tell you how close to the edge of the pixel the interaction occurred)
  - The angle of deflection due to the Lorentz effect has been found to increase as a function of radiation damage
- Hit reconstruction efficiency is very high: 99.5% (99%) in pixels (strips)
- Total radiation length ranges from  $0.5\times$  to  $2 \times X_0$ 
  - Lowest at low  $\eta$

### 8.1.1 Inner pixel detector

- Detector specification:
  - 66 million silicon pixels
  - $100 \mu\text{m} \times 150 \mu\text{m} \times 285 \mu\text{m}$  pixels
  - Three barrel layers at radii of 4.3, 7.2, and 11 cm
  - Two endcap disk layers at  $z$  of 35 and 46 cm
  - Position of layers guarantees at least 3 hits (not accounting for detector efficiency) for  $|\eta| < 2.5$
- Flux of particles is  $10^6 \text{ cm}^{-2}\text{s}^{-1}$
- Hit reconstruction
  - Readout threshold is 3.2k electron-equivalent charges
  - Offline, define a pixel cluster as adjacent (either sharing a side or corner) pixels containing at least 4k electrons

- MIP typically deposits 20k electrons
- Position of particle within cluster determined by using charge distribution
- Resolution of hit is  $\sigma_{r\phi} \sim 10 \mu\text{m}$  and  $\sigma_z \sim 30 \mu\text{m}$
- Radiation damage can be assessed and corrected for by looking at the mean response as a function of time
- Occupancy is typically  $10^{-4}$ - $10^{-3}$  per channel
  - Particle density is higher than in the outer detector, but occupancy is lower because of granularity

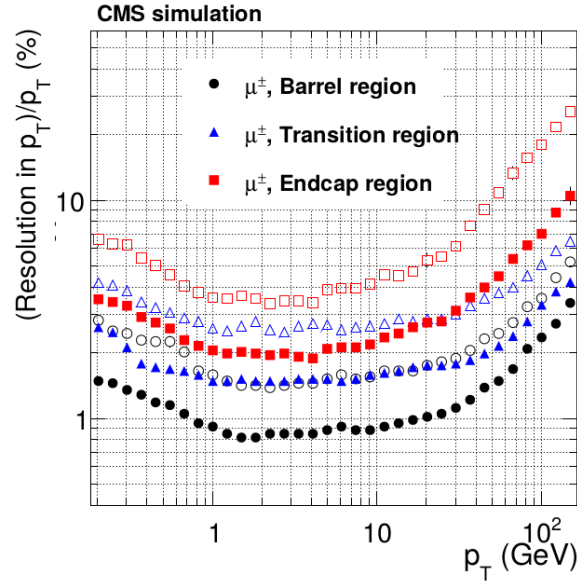
### 8.1.2 Outer strip detector

- Detector specification:
  - 9 million p-type strips embedded into a n-type bulk (thickness  $\sim 320$ - $500 \mu\text{m}$ )
  - Like the inner detector, consists of multiple barrel and endcap disk layers
  - About half the layers are 1D (i.e. provide only  $r\phi$  measurement) and the other half are 2D (giving 3D position measurement)
  - Ranges from 25 cm to 110 cm in  $r$  and up to 120 cm (280 cm) in  $z$  in the barrel (endcap)
  - Strip lengths are 10-20 cm. Strip pitch (spacing) is 80-205  $\mu\text{m}$ 
    - \* Things are finer in the innermost layers
- Occupancy ranges from  $10^{-3}$  to  $10^{-2}$
- Use charge-weighted average to determine position of hit
  - Spatial resolution is therefore  $\sim 20$ - $50 \mu\text{m}$

### 8.1.3 Track reconstruction

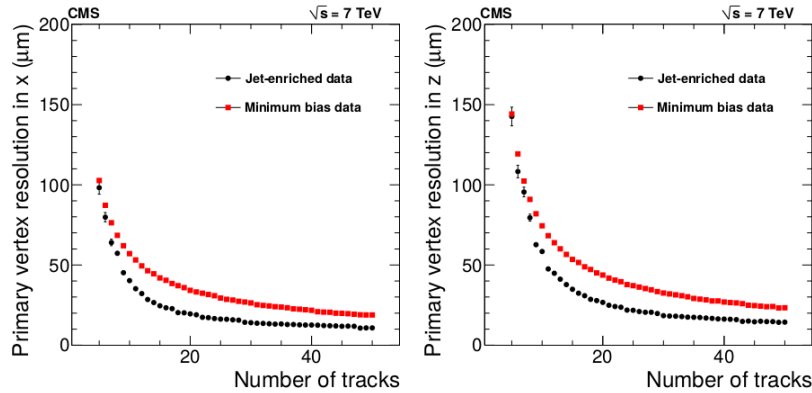
- Iteratively do pattern recognition and track fitting using a combinatorial Kalman filter
  - First look for high  $p_T$  tracks (easiest to reconstruct), then remove these hits and repeat until all hits are associated with a track or classified as noise
  - 6 such iterations are done at CMS
- Each iteration does 4 things:
  - First, generate track seeds using collections of 2-3 hits in the pixel detector and estimate trajectory parameters from this seed
  - Extrapolate the track from the seed using a Kalman filter and search for hits consistent with the extrapolation
  - Run a track fitting procedure to get best estimate of trajectory parameters and covariance matrix
  - Discard tracks that fail quality requirements (i.e. too many missing hits, bad  $\chi^2, \dots$ )
- The trajectory parameters take into account several effects:
  - Curvature due to  $\vec{B}$ -field
  - Change in path from multiple scattering (can be difficult to do if angle is large for a high  $p_T$  track)
  - Change in curvature due to  $dE/dx$
- Electron tracking

- Electrons lose a lot of energy in tracker due to bremsstrahlung: up to 70%. Energy loss is very non-Gaussian
- Use additional ECAL info to build electron tracks
  - \* For example, look for ECAL clusters from the bremsstrahlung photons
- Tracking efficiency is  $\gtrsim 90\%$  ( $\gtrsim 99\%$ ) for electrons and pions (muons) if  $p_T > 10$  GeV is required
- Resolution on  $p_T$  ranges from 1% to 10%, as a function of  $p_T, \eta$ :



#### 8.1.4 Vertex reconstruction

- Primary vertex resolution is  $\sim \mathcal{O}(10)$   $\mu\text{m}$  and depends on the number of tracks:



- Efficiency is  $> 0.995$  if at least 3 tracks are present
- Similarly, can use tracks with high impact parameter to reconstruct secondary vertices (decays of  $B$  mesons,  $K^0$ ,  $\gamma \rightarrow e^-e^+$ ). Resolution is similar to PVs

## 8.2 Electromagnetic calorimeter

- Two components: barrel ( $|\eta| < 1.479$ ) and endcap ( $1.653 < |\eta| < 3.0$ )
  - Preshower coverage for endcap ends at  $|\eta| < 2.6$

- Made out of lead-tungstate crystals ( $\text{PbWO}_4$ )
  - $X_0 = 0.89$  cm and  $R_M = 2.2$  cm. These are quite small
  - Response times are  $\tau_f = 10$  ns and  $\tau_s = 25$  ns
    - \* This is an order of magnitude better than other inorganic scintillators
  - Emits light at 420 nm
- ECAL is a homogeneous calorimeter: single crystals that act as the absorber and detector
  - Advantage: very good energy resolution
  - Disadvantage: expensive and no longitudinal shower information

### 8.2.1 Barrel configuration

- 61k crystals of dimension  $R_M \times R_M \times 26X_0$
- Each crystal has dedicated APD, operated in linear mode (gain of 50)
- QE of APDs is 80%

### 8.2.2 Endcap configuration

- 14k crystals of dimension  $1.3R_M \times 1.3R_M \times 25X_0$
- Each crystal has a dedicated vacuum phototriode, operated in linear mode (gain of 10)
  - QE is 20%
  - Use VPT instead of Si APD because of radiation hardness requirements
  - Response is very fast: 1 ns
  - Honestly, there are some things about VPT operation that I do not understand. Yutaro was also unsure. Probably unimportant...
- Preshower detector
  - At high  $\eta$ , a  $\pi^0 \rightarrow \gamma\gamma$  decay might be boosted enough that the photons overlap in the ECAL
  - The preshower is two layers of Pb+Si detectors with a spatial resolution of 2 mm  $\Rightarrow$  can distinguish  $\gamma$  from  $\gamma\gamma$
  - This detector is right before endcap ECAL

### 8.2.3 Electron and photon reconstruction

- Most particles deposit all energy within  $3 \times 3$  box of crystals
- Particles are seeded using ECAL superclusters
  - Start with some pre-defined seed of crystals (such as one high-energy crystal)
  - Then add adjacent crystals to the supercluster if they also have high energy
- Center of the cluster is defined by log-weighting the energy
- For photons, the energy is defined by looking at a  $5 \times 5$  cluster
- Electron-initiated showers are wider due to brem, so the energy is defined as the total energy of the super-cluster



- Distinguishing between a  $e$  and  $\gamma$  (or charged hadrons) can be done using the  $\eta$ - $\phi$  shape of the shower
  - Also only an electron should have 1 track, conversion have 2 tracks, charged hadron have HCAL deposit, etc...

### 8.2.4 Energy resolution

- The energy resolution in the barrel is:

$$\frac{\sigma_E}{E} = \frac{2.8\%}{\sqrt{E [\text{GeV}]}} \oplus \frac{0.128}{E [\text{GeV}]} \oplus 0.3\% \quad (32)$$

It is slightly worse in the endcap

- ECAL is instrumented with lasers of known energy to constantly monitor resolution
- Photon energy resolution is  $\sim 1$  GeV at  $p_T = 100$  GeV
- Resolution of  $m_{\gamma\gamma}$  in Higgs discovery was  $\sim$  GeV. This is determined by:
  - Energy resolution of each photon
  - Position resolution of superclusters (so opening angle can be measured)

## 8.3 Hadron calorimeter

- 4 components:
  - $|\eta| < 1.39$ : Barrel
  - $1.30 < |\eta| < 3.00$ : Endcap
  - $2.85 < |\eta| < 5.19$ : Forward
  - $|\eta| < 1.30$ : Outer
- Note that, unlike the ECAL, there is no gap until the end of the detector
  - Necessary for good  $\cancel{E}_T$  resolution, since most particles in an event are hadrons
- HO is outside the solenoid; other components are inside
  - Inside solenoid reduces material budget before detector  $\Rightarrow$  better energy resolution
  - However, limited size of solenoid  $\Rightarrow$  thickness of HB is only  $\sim 6\lambda_I$  (where  $\lambda_I$  is the nuclear interaction mean free path)
  - HO is used to extend this
- Light collection done using hybrid photodiodes

### 8.3.1 HCAL Barrel

- Consists of 1 steel layer, 14 brass layers, and another steel layer
  - $\lambda_I$  for brass is 16.4 cm
  - Total depth is equivalent to  $5.9\lambda_I$
  - Each brass layer is  $\sim 50$  mm thick
  - Absorber layers are interleaved with plastic scintillator

- Segmented into  $\eta$ - $\phi$  towers of  $0.087 \times 0.087$  radians
- Small thickness  $\Rightarrow$  stochastic term dominates energy resolution:

$$\left(\frac{d\sigma_E}{dE}\right)_{\pi^0} \approx \frac{0.9}{\sqrt{E} [\text{GeV}]} \quad (33)$$

### 8.3.2 HCAL Endcap

- Also brass and steel
  - Total depth is equivalent to  $10\lambda_I$
- Also segmented into  $\eta$ - $\phi$  towers of  $0.087 \times 0.087$  radians
- Pion energy resolution:

$$\left(\frac{d\sigma_E}{dE}\right)_{\pi^0} \approx \frac{1}{\sqrt{E} [\text{GeV}]} \quad (34)$$

### 8.3.3 HCAL Forward

- Iron absorbers interleaved with quartz
  - Total depth is equivalent to  $10\lambda_I$
  - Collect Cerenkov light from quartz
- Segmented into  $36 \times 13$  towers in the  $\phi \times \eta$  plane

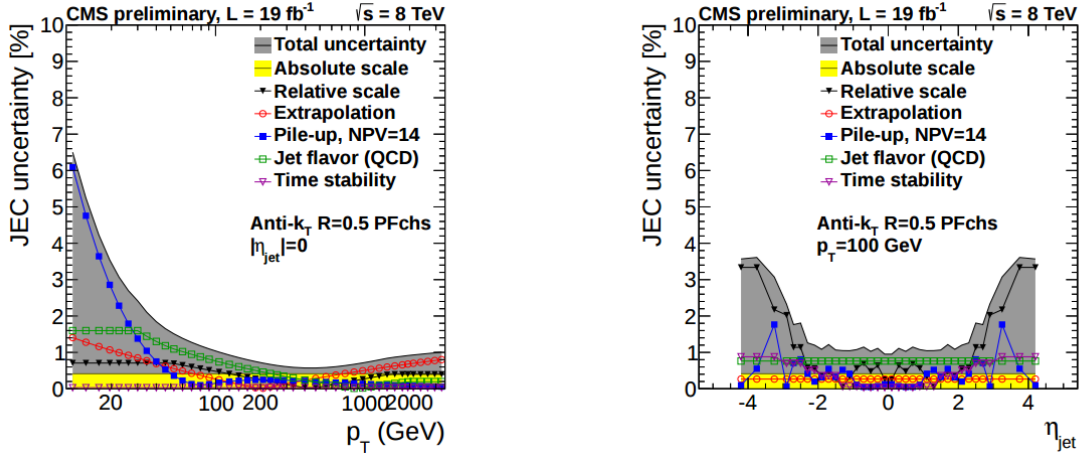
### 8.3.4 HCAL Outer

- Uses the solenoid and first yoke layer (mostly aluminum and iron, respectively) as absorbers
  - Total depth is equivalent to  $10\lambda_I$
  - Layer of scintillator after each absorber
- Pion energy resolution:

$$\left(\frac{d\sigma_E}{dE}\right)_{\pi^0} \approx \frac{1.2}{\sqrt{E} [\text{GeV}]} \quad (35)$$

### 8.3.5 Jet energy resolution

- The reconstructed objects of the HCAL are jets
  - Reconstruction uses tracking and ECAL information as well
- Uncertainty in  $p_T$  is at worst 7% and is better than 1% for central, high  $p_T$  jets:



- Calibrating jet energy scale is very important as it controls the uncertainty on the  $\cancel{E}_T$

## 8.4 Magnet and return yokes

- Magnet is a solenoid generating a 3.8 T field inside
- Coil is a superconducting alloy. Maintained at 4 K using LiHe
- It uses a lot of aluminum to stabilize the superconducting coil
- Superconducting coil is NbTi
- Radius of solenoid is 3 m
- Outside the solenoid:
  - $\vec{B}$ -field is in the opposite direction and has strength  $\sim 2 \text{ T}$
  - $\vec{B}$ -field is guided using 4 iron return yokes

## 8.5 Muon detectors

- Magnet return yokes are used to shield muon detectors from punch-through hadrons
- Three components:
  - Drift tubes:  $|\eta| < 1.2$
  - Cathode strip chambers:  $0.9 < |\eta| < 2.4$
  - Resistive plate chambers:  $|\eta| < 2.1$

### 8.5.1 Drift tubes

- 240 drift tube chambers over  $|\eta| < 1.2$
- Organized radially in 4 stations, with the return yoke interspersed
  - Each station has multiple drift tubes in it
  - Note these station also have RPC detectors (discussed below)
- Each station has three superlayers of DTs:

- 2 superlayers consisting of 4 layers each that the  $\phi$  position
- 1 superlayer consisting of 4 layers that gives the  $z$  position
- Drift gas is argon (85%) and  $\text{CO}_2$  (15%)
- Maximum drift time is 400 ns
  - Resolution on drift time is 1 ns
- Each chamber (i.e. layer) has a spatial resolution 100  $\mu\text{m}$  in the value of  $\phi$ - $z$  plane

### 8.5.2 Resistive plate chambers

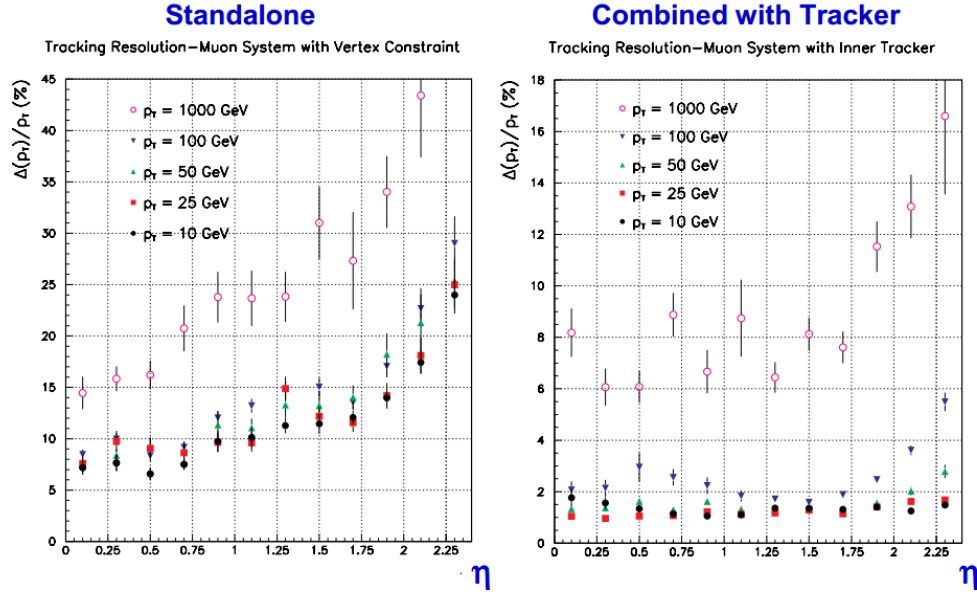
- 612 RPCs
  - 6 stations in the barrel
  - 4 stations in the endcaps
- Operated in avalanche mode
- Gap width is 2 mm
- Gas is mostly  $\text{C}_2\text{H}_2\text{F}_4$
- Timing resolution is very good: 3 ns

### 8.5.3 Cathode strip chambers

- Used in the barrel because it can handle higher fluxes
- Total of 6 endcap stations
- Essentially a proportional counter, except each chamber is instrumented with multiple anode wires and cathode strips
  - Anodes and cathodes are perpendicular to each other
- Muon creates a primary ionization which induces an avalanche. Ions move to cathode and electrons to anode, giving 2D spatial reconstruction
- Spatial resolution is 100  $\mu\text{m}$  and timing resolution is 3 ns

### 8.5.4 Muon reconstruction

- Can identify a standalone muon (using just the muon chambers) or a global muon (adding tracker info)
  - Note tracker gives complementary information, since  $\vec{B}$ -field changes direction
  - Below 200 GeV, tracker dominates accuracy, since multiple scattering in solenoid and yoke messes up measurement in muon chambers
- Global muon reconstruction efficiency is  $\gtrsim 97\%$
- Global muon  $p_T$  uncertainty is less than 1% for  $p_T < 100$  GeV:



## 8.6 Triggering and DAQ

- LHC Run II luminosity is  $10^{34} \text{ cm}^{-2}\text{s}^{-1}$  and inelastic  $pp$  scattering cross section is 70 mb, so the event rate is  $\sim 10^9/\text{s}$
- Each bunch crossing has an average of 22 overlaid events. Bunch crossing rate is 40 MHz
- If each event is  $\sim 1 \text{ MB}$ , then the data output is over 1 TB each second
  - Way too high to write out using existing implementations (although I believe DarkLight is aiming for this order of magnitude)
- Two stages: L1 and HLT
- Level 1 trigger system
  - Uses muon and calorimeter information to select interesting events
  - Can construct primitives like muons, electrons, photons; can also measure global variables like  $E_T$ ,  $H_T$ ,  $\cancel{E}_T$ 
    - \* Use faster, but less accurate, reconstruction methods than what is used offline
  - Three components:
    - \* Global calorimeter trigger
    - \* Global muon trigger
    - \* Global trigger (takes info from GCT and GMT)
  - Reduces event rate from 40 MHz to 50 kHz
  - Functions by keeping events in buffer (“front-end pipeline”) for a few microseconds. Event processing time is about 1 microsecond
  - Calculation is done online using FPGAs
  - Proposals for future is to add tracking information to L1 trigger: use fast pattern recognition to reconstruct track primitives for triggering
- High Level Trigger system
  - Each HLT path is “seeded” by a L1 trigger

- \* For example, a HLT path that looks for  $b$ -tagged jets would be seeded by an L1 trigger with requirements on  $H_T$
- Reduces event rate down to  $\mathcal{O}(100)$  Hz
  - \* At most 90% is used for actual physics; rest is dedicated for detector calibration
- Decisions are made using information from all detector components
- However, reconstruction is only partial, to reduce CPU time
  - \* Objects are reconstructed following objects that are identified by corresponding L1 trigger
- Three levels within HLT:
  - \* Level 2.0: still no tracking information. Does stuff like construct ECAL superclusters.  $\mathcal{O}(100)$  ms
  - \* Level 2.5: primitive tracking and vertexing using only pixels.  $\mathcal{O}(10)$  ms
  - \* Level 3.0: using full tracker.  $\mathcal{O}(100)$  ms
- Average processing time ranges from 50 ms (jets+ $\cancel{E}_T$ ) to 700 ms (muons)

## Appendices

### A Bibliography

The CMS Collaboration, *Description and performance of track and primary-vertex reconstruction with the CMS tracker*. [arXiv:1405.6569](#)

The CMS Collaboration, *The Magnet Project Technical Design Report*. CERN/LHCC 97-10

The CMS Collaboration, *Performance of CMS muon reconstruction in pp collision events at  $\sqrt{s} = 7$  TeV*. [arXiv:1206.4071](#)

The CMS Collaboration, *Energy calibration and resolution of the CMS electromagnetic calorimeter in pp collisions at  $\sqrt{s} = 7$  TeV*. [arXiv:1206.2016](#)

The CMS Collaboration, *Performance of jets at CMS*. 2015 J. Phys.: Conf. Ser. 587 012004

The CMS Collaboration, *Operation and performance of the CMS tracker*. [arXiv:1402.0675](#)

The CMS Collaboration, *The CMS High Level Trigger*.

The CMS Collaboration, *The CMS ECAL performance with examples*. 2014 JINST 9 C02008

Leo, W. R., *Techniques for Nuclear and Particle Physics Experiments*. Second Revised Edition

PDG Particle Review, *Passage of Particles Through Matter*. 2014 edition

PDG Particle Review, *Particle Detectors at Accelerators*. 2015 edition